Modelling of shell and tube heat exchangers

John Hellborg

2017-01-10

A thesis presented for the degree of
Master of Science in Engineering - Engineering Physics

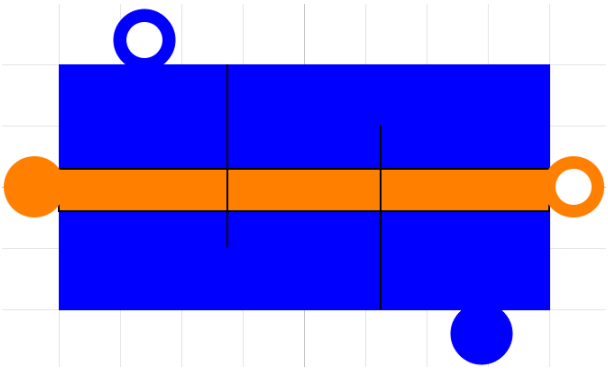

Division of Heat Transfer
Lund University, LTH, in collaboration with Modelon AB
Sweden

Abstract

In this master thesis Modelica models for shell and tube heat exchangers was developed. The modelling focused on two configurations specifically; the TEMA E shell and tube heat exchanger with single-phase flow on the shell side and the TEMA G shell and tube heat exchanger with condensation on the shell side.

The finite volume method (FVM), based on the models in the Modelon Base Library and the Heat Exchanger Library, was used. Correlations for the heat transfer coefficient and pressure drop were based on two different version of the Delaware method, the Chisholm two-phase multiplier and the method developed by Honda. Full coverage of the equations for all of the methods are given in the report.

The models were tested in simulations and the qualitative analysis based on these simulations showed several effects that agreed with the theoretical predictions.

1 Acknowledgements

Many people contributed to the progress of this master thesis. Firstly, I want to express my gratitude to my supervisors at Modelon AB; Anders Nylén, Katrin Prölss and Pieter Dermont. Both their insight and their commitment to the subject were irreplaceable. The rest of the Modelon staff deserve credit too, for their kind welcoming, their Dymola introduction course and serious approach to the master thesis.

My supervisor at LTH, Martin Andersson, is responsible for the theoretical insight on which the thesis was based. Both through valuable guiding during the progress thesis and through the course that inspired me to study heat exchangers, for which he was course responsible and lecturer. At the division of Heat Transfer great help was also received from Prof. Bengt Sundén and Zan Wu.

Further on I want to thank the co-operators from other companies who all have contributed with experimental data on shell and tube condensers. Elisabeth Wahlström at Perstorp Oxo AB, Oleg Savin at OSC VNIIKHOLODMASH-HOLDING as well as Eric Lillberg and Nicolas Edh at Vattenfall AB.

Finally, I want to show my appreciation for the support from home. Both from Emilia and from the rest of my family.

Nomenclature

Physical properties

α	Heat transfer coefficient	W/Km^2
β	f_B calibration factor	1
Δp	Pressure drop	Pa
Δp_{ideal}	Ideal pressure drop in cross-flow section	Pa
$\Delta p_{w,ideal}$	Ideal pressure drop in window section	Pa
$\dot{m}$	Mass flow rate	kg/s
Γ	Fluid properties correction factor	1
ϕ	Two-phase multiplier	1
ε	Friction factor	1
a, a_{1-4}	Coefficients in the Delaware heat transfer method	1
b, b_{1-4}	Coefficients in the Delaware pressure drop method	1
C_J	J_B calibration factor	1
C_R	R_B calibration factor	1
F	LMTD correction factor	1
f	Friction factor	kg/s
f_A	Tube arrangement correction factor	1
f_B	Tube bundle bypass correction factor	1
F_c	Fraction of the tubes in cross-flow section	1
f_G	Geometry correction factor	1
f_L	Baffle leakage correction factor	1
f_P	Boundary layer correction factor	1
f_W	Shell correction factor	1
$f_{a,l,f}$	In-line laminar arrangement factor	1
$f_{a,l,v}$	Staggered laminar arrangement factor	1
$f_{a,t,f}$	In-line turbulent arrangement factor	1
$f_{a,t,v}$	Staggered turbulent arrangement factor	1
$f_{z,l}$	Laminar correction factor	1
$f_{z,t}$	Turbulent correction factor	1
G	Mass flux	kg/sm^2
j	Colburn j-factor	1

J_B	Tube bundle bypass flow correction factor	1
J_L	Baffle leakage correction factor	1
J_R	Laminar flow correction factor	1
J_R	Window section correction factor	1
J_S	Unequal baffle spacing correction factor	1
$LMTD$	Log-mean temperature difference	K
m	Mass	kg
n_2	R_S calibration factor	1
p	R_L calibration factor	1
p	Pressure	Pa
Q	Heat flow rate	W
q	Heat flux	W/m^2
R_B	Tube bundle bypass flow correction factor	1
R_L	Baffle leakage correction factor	1
R_S	Unequal baffle spacing correction factor	1
R_w	Thermal resistance	K/W
T	Temperature	K
U	Overall heat transfer coefficient	W/m^2K
u	Velocity	m/s
Fluid properties		
η	Dynamic viscosity	kg/sm
λ	Thermal conductivity	W/Km
ρ	Density	kg/m^3
c_p	Specific heat capacity	J/kgK
Dimensionless numbers		
Gr	Grashof number	1
Nu	Nusselt number	1
$Nu_{0,bundle}$	Ideal tube bundle nusselt number	1
$Nu_{0,lam}$	Laminar nusselt number	1
$Nu_{0,turb}$	Turbulent nusselt number	1
$Nu_{l,0}$	Ideal nusselt number	1
Pr	Prandtl number	1

Re	Reynold's number	1
Geometrical parameters		
$\delta_s b$	Shell-to-baffle distance	m
$\delta_t b$	Tube-to-baffle distance	m
ϵ	Roughness factor	m
ϕ	Void fraction	1
θ_{ctl}	Center tube limit angle	rad
θ_{ds}	Diameter-shell angle	rad
A	Area	m^2
A_b	Tube bundle bypass area	m^2
$A_i n$	Inlet cross-sectional area	m^2
B	Baffle distance	m
B_c	Fractional baffle cut	1
B_{in}	Enter section baffle distance	m
B_{out}	End section baffle distance	m
D	Diameter	m
D_e		m^2
D_i	Inner tube diameter	m
D_o	Outer tube diameter	m
D_{ctl}	Center tube limit diameter	m
D_{otl}	Outer tube limit diameter	m
e	Shortest connection length	m
F_w	Tubes in window section fraction	1
L	Length	m
L_e	Total shortest connection length	m
m	e section calibration factor	1
n_1	J_S calibration factor	1
n_b	Number of baffles	m^2
N_c	Number of tube rows in cross-flow section	1
n_t	Number of tubes	1
n_w	Number of tubes in window section	1
N_{ct}	Total number of tubes crossed	1

N_{cw}	Number of tubes crossed in window section	1
N_{ss}	Number of sealing strips	1
n_{tubes}	Vector where the i$^t h$ element is the number of tubes in the i$^t h$ row	1
NTP	Number of tube passes	1
P_L	Longitudinal tube pitch	m
P_T	Transverse tube pitch	m
P'_T	Modified transverse tube pitch	m
R_B	Area ratio	1
r_i	Inner tube radius	m
r_l	Area ratio	1
r_o	Outer tube radius	m
R_Q	Area ratio	1
r_s	Area ratio	1
r_{ss}	Sealing strip ratio	1
S_b	Tube bundle bypass area	m^2
S_e	Shortest connection area	m^2
S_m	Cross-flow area	m^2
S_w	Window flow area	m^2
S_{sb}	Shell-to-baffle area	m^2
S_{tb}	Tube-to-baffle area	m^2
V	Volume	m^3

Subscripts

c	Cross-flow section
e	Enter/end section
grav	Gravitational
liq	Liquid
s	Shell side
t	Tube side
turb	Turbulent
vap	Vapor
w	Wall/Window section

Contents

2 Introduction

2.1 Overview

This report is the documentation of the master thesis executed by John Hellborg at the department of Heat transfer at Lund Institute of Technology and at Modelon AB. The purpose of the thesis was to develop models for shell and tube heat exchangers. The models were implemented in the modelling language Modelica and many of them were based on previously implemented models and modelling ideas in some of the Modelica libraries developed by Modelon. The modelling and the simulations were done in the Modelica tool Dymola.

There are several different types of shell and tube heat exchangers, see more about this in section 2. In this thesis two specific configurations (versions) were considered. The first was the TEMA E shell and tube heat exchanger with single-phase flow on the shell side. The second was the TEMA G shell and tube heat exchanger with condensation on the shell side. For simplicity the first one is often referred to as the shell and tube heat exchanger and the second is referred to as the shell and tube condenser (even though both are versions of a shell and tube heat exchanger).

The objective of the thesis was to implement as generic models as possible that could be used in dynamic simulations. The assumptions made in the modelling were therefore minimized and as much flexibility as possible was left to the user of the models. The main modelling strategy was to implement models for each of the components in a shell and tube heat exchanger and assembling them into complete heat exchangers. The main computational approach was the finite volume method (FVM).

2.2 Motivation

Since the beginning of the computer era more and more physical phenomena have been modelled in order to simulate instead of experimenting. Experiments are often costly since they require the need of experimental setups, such as physical components and measuring equipment. Simulation on the other hand only requires a computer, a simulation tool and a model.

For a shell and tube heat exchanger the advantages of simulations are clear. The product is expensive and technical to construct. To test different models or to do dimensional analysis simulations are very important. Since the middle of the 20^{th} century correlations for shell and tube heat exchangers have been developed. The first methods were designed for steady-state calculations and was not applicable for dynamical simulations. As the power of computer increased the complexity of simulation tools and models also was enhanced. Today Computational Fluid Dynamics (CFD) is implemented in several tools, the models that can be created are complex and the simulations are both more accurate and more time-consuming than the early developed methods. By using complicated meshing and solving the differential equations of fluid mechanics the user can receive an approximation of the solution based on fundamental physics. But to what cost?

To avoid the costly meshing another modelling approach was required. The finite volume method offers a way to model complex physical systems using correlations. Using this method models can be created that offers the user to change the geometry and settings of the heat exchanger using simple parameters. Since the meshing could be done simply, the simulation time was low which always is preferable, especially when the shell and tube heat exchanger is a part of a larger system, for example a car.

2.3 Modelon AB

Since the foundation in 2005 Modelon AB has significantly contributed in the field of modelling. The employees are located in USA, Japan, Sweden and Germany. Some of the various tasks at Modelon are the work with the development of commercial Modelica libraries for various fields, for example thermal power and vehicle dynamics and consulting of Modelica modelling. Modelon gives modelling courses, for example an introduction course to Dymola, a simulation tool of which Modelon is a reseller.

Modelon also develop Functional Mock-up Interface FMI which is an open-standard for model exchange between different simulation tools and work for the progression of Modelica, partly from several places in the board of the Modelica Association.

2.4 Thesis outline

2.4.0.1 Introduction The report begins in an introduction where the subject and the report is introduced. The introduction gives an overview of the work done during the master thesis and what tools that were used. Background and motivation for the thesis is presented in order to give the reader a perspective on what the thesis can contribute with and why the thesis was necessary. Following the motivation, a presentation of Modelon (the company where the thesis was conducted) is done.

2.4.0.2 Theory The theoretical background and developed science that was used in the thesis is presented in section 3. The first part of section 3 explains heat exchangers in general. What is a heat exchanger? Where can it be used? What properties are important for heat exchangers in general? Such questions are answered in section 3.1. Since only shell and tube heat exchangers were considered in this thesis a more thorough description of that type of heat exchanger is given in section 3.2. The different components are explained and ways of classifying shell and tube heat exchangers are presented. The types of heat exchangers modelled in the thesis are focused on but to give the reader a view of what was never implemented, other variations of shell and tube heat exchanger are mentioned as well. The models were implemented in Modelica using the tool Dymola. Each of these are described in section 3.3. Focus in the description of Modelica lies on the differences and similarities between Modelica and more classical programming languages, such as Python. The text about Dymola was written in order to give the reader the important aspects of the tool for the thesis, such as how the modelling can be done. Section 3.4 is a theoretical literature study on fluid dynamics. In this section the research and the theories used in the thesis are presented to give a theoretical foundation for the modelling and the discussion of the simulated results. One section is written only for two-phase flow to describe the difficulties in modelling and computation of it. The following sections describe the scientific advancements concerning shell and tube heat exchangers, mainly about the modelling of pressure drop and heat transfer coefficient.

2.4.0.3 Modelling The modelling done during the thesis is documented in section 4. The section begins with an overview of the models created. Following, the major components are presented one by one. Each of the sections 4.1-4.6 have are presented with a list of assumptions made for the model and a text explaining why it was necessary to do these assumptions and justifying them. The sections 4.1-4.6 also include a design part where the way of modelling is described and discussed. For the models where it is applicable the method for heat transfer and pressure drop calculation are presented in their own subsections. This is where the complex and large systems of equations are given. Because of the size of some of the methods the number of equations is high, these subsections are therefore long and are mainly written for the reader who wants to replicate some of the models of do models based on the same methods.

2.4.0.4 Simulations A part of the thesis was to test the models using simulations. The declaration of each simulation can be found in section 5. The intent behind this section was to describe the simulations well enough for someone else to execute the same simulations and verify the results. The section is divided into two parts, one for each of the two types of shell and tube heat exchangers modelled in the thesis. Each of these parts are divided into smaller parts for each simulation.

2.4.0.5 Results The results of the simulations are presented in section 6. The structure of section 6 is the same as of section 5 in order for the reader to easily know which simulation description that belong to which result.

2.4.0.6 Discussion The modelling and the simulated results are discussed in section 7. This section is also divided into one section for each type of shell and tube heat exchanger, as section 5 and 6. Assumptions, strengths and weaknesses of the models are analyzed. The most important conclusions are collected in section 7.3 and ideas for future work are given in section 7.4.

All references used in the report are given in section 8.

3 Theory

3.1 Heat exchangers

A heat exchanger is a device in which heat is transferred from one fluid to another. Heat exchangers are used in many various applications. One example is a car, where heat from the air around the engine is transferred to the air inside the car. In this way the car is warmed up and the engine is not overheated. Another example is ventilation. The hot air going out of a building transfers some of its heat to the cold air entering the building [1].

There are some parameters that are important for all heat exchangers. Since the purpose of the heat exchanger is to transfer energy, the heat flow rate, Q, is always of great interest. Equation 1 describes how the heat flow can be expressed. The same equation also shows what properties that are significant for the heat flow. α, heat transfer coefficient (in some literature the notation for heat transfer coefficient is h), A, heat transfer area and ΔT, the temperature difference, are the variables that should be maximized in order to get as high heat flow rate as possible.

$$Q = \alpha \cdot A \cdot \Delta T \tag{1}$$

Equation 1 is a general equation for convective heat transfer [2]. When working with heat exchangers it is often more applicable to work with equation 2 [2]. Equation 2 calculates the overall heat flow rate for the entire heat exchanger instead of the local heat flow as in equation 1. U is the overall heat transfer coefficient. The equation for this property is different for different heat exchangers but the equation for a shell and tube heat exchanger is presented in equation 3 [3]. In equation 3, α_s and α_t are the heat transfer coefficients on the shell side and the tube side respectively. A is the heat transfer surface of the entire heat exchanger. F is the $LMTD$ correction factor and depends on the flow arrangement (see below). $LMTD$ stands for Log-Mean Temperature Difference and is presented in equation 4, ΔT_a and ΔT_b are the temperature differences between the two fluids in the different sides of the heat exchanger [2].

$$Q = U \cdot A \cdot F \cdot LMTD \tag{2}$$

$$\frac{1}{U} = \frac{D_o}{D_i \alpha_t} + \frac{D_0 ln(D_o/D_i)}{2\lambda_w} + \frac{1}{\alpha_s} \tag{3}$$

$$LMTD = \frac{\Delta T_b - \Delta T_a}{ln(\Delta T_b / \Delta T_a)} \tag{4}$$

Generally, the fluids will not travel through the heat exchanger spontaneously, they have to be pumped. How much energy that is needed to pump the fluids through the heat exchanger is determined by the pressure drop, Δp. Other variables that are interesting for all heat exchangers are the mass flow rate of the two fluids.

Heat exchanger can be classified according to design configuration, phases of the fluids and flow arrangement. Common design configurations are the shell and tube heat exchanger and the plate heat exchanger. When classified according to phase, heat exchangers can be divided into condensers, evaporators, one-phase heat exchangers and radiators. There are three main flow arrangements: Counter-flow, co-flow and cross-flow. The different arrangements can also be combined [2]. For a counter-flow heat exchanger the $LMTD$ correction factor $F = 1$ and for other configurations the value is $0 < F \leq 1$.

In this thesis the shell and tube heat exchanger was modelled. Condensers and one-phase heat exchangers were both considered. Counter-flow, co-flow and cross-flow were implemented.

3.2 Shell-and-tube heat exchangers

A common heat exchanger is the shell-and-tube heat exchanger, see example in figure 1. In this kind of heat exchanger one fluid flows inside a tube bundle and the other fluid flows in a shell surrounding this tube bundle. Shell-and-tube heat exchangers are often used in process industries such as oil refineries [2, 4]. A few properties make the shell-and-tube heat exchanger favorable. The geometry allows for high pressure and flexibility concerning phases as well as the possibility to use finned tubes for increased heat transfer, which makes the shell and tube heat exchanger usable in many applications. A disadvantages of the shell-and-tube heat exchanger is the risk of tube vibrations caused by the flow [2], read more in chapter 3.2.1.3.

3.2.1 Components

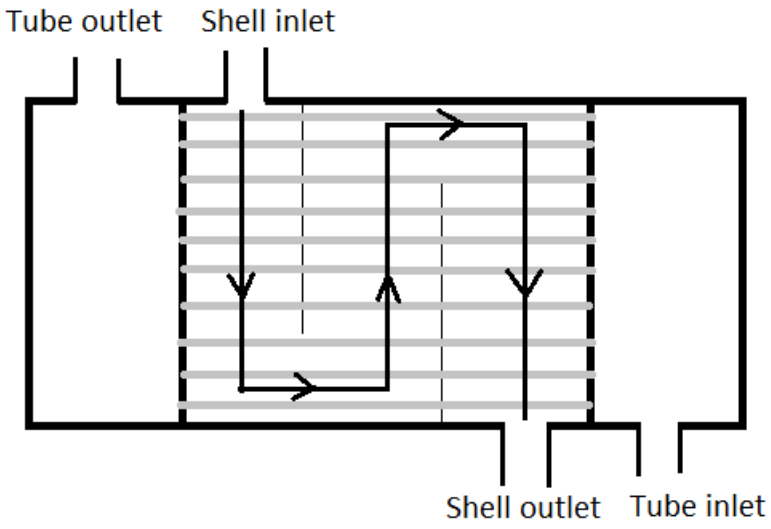

Figure 1: Schematic example of a shell-and-tube heat exchanger

To visualize the different components an example of a shell-and-tube heat exchanger is used, see figure 1.

3.2.1.1 Tubes The tubes in the shell-and-tube heat exchanger make up a tube bundle in which one of the fluids flows. In figure 1 the tubes are drawn as thick, grey, horizontal lines. The tubes are often cylindrical and takes the fluid from the front-head to the end-head [5]. In some heat exchangers the tubes make more than one pass through the shell. In figure 1 a single-pass shell and tube heat exchanger is shown.

The fluid in the tubes transfer heat to the tube wall which separates the tube fluid from the shell fluid. The tube wall typically consists of a metal, but can also be made from plastics or ceramics depending on application [5].

Some rules of thumb exist concerning the choice of which fluid should be on the shell side and the tube side respectively. The more robust tubes should preferably hold the fluid with the highest temperature and pressure. This argument is also strengthened by the fact that the tube side fluid only affects the material in the tube wall and therefore it is only the tube wall that needs to be strong enough to endure the pressures from the tube side fluid. The ideal fluid for the tube side can further be described as the least viscous and the one with the highest mass flow rate [2].

The primary defining parameters of the tubes are the inner and outer diameter (or hydraulic diameter if the tubes are not cylindrical) and the tube length. Interesting variables in a tube is the inlet- and outlet temperatures as well and the heat flow rate and the pressure drop. Since the heat flow rate is important then so is the heat transfer coefficient used to calculate the heat flow rate. The heat transfer coefficient and the pressure drop is generally dependent on the mass flow rate which makes this another important parameter.

3.2.1.2 Shell The fluid on the shell side of a shell and tube heat exchanger travels from the shell inlet to the shell outlet. Guided by baffles (see below) it crosses the tubes for the heat transfer to occur, see figure 1.

Corresponding to the reasoning on which fluid should be in the tubes the ideal shell side fluid is characterized with low pressure (the complex flow would otherwise tear on the shell wall, the baffles and the tube walls), low temperature, high viscosity and low mass flow rate [2].

Normally the shell is cylindrical and made of metal [5]. In this case a shell diameter and a length are defining parameters. The rest of the geometrical definition of a shell is dependent on the type of shell, see chapter 3.2.2. The complex geometry of the shell and tube heat exchanger makes the calculations of heat transfer and pressure drop complex. The fact that there are many different types of designs also makes the modelling process more complicated by increasing the difficulty in making a generic shell model.

3.2.1.3 Baffles Shell and tube heat exchanger have baffles for two main reasons. The first is to give stability to the tubes. Without baffles the tube (that can be several meters long) would risk much to high flow-induced vibrations due to the fluctuating flow on the shell side. These vibrations would damage the heat exchanger. With the baffles the distance between two points where the tubes are fixed decreases, making the tubes more stable [5].

The other use of baffles is to guide the shell side flow through the shell. As seen in figure 1 the baffles create cross-flow instead of pure counter- or co-flow. Cross-flow reduces the temperature difference between the different tubes and it decreases the thermal stress [5]. The baffles also increase the turbulence on the shell side leading to an enhanced heat transfer [5].

There is a downside of having baffles. The fact that they guide the shell side fluid explains that the baffles work as obstacles for the flow, increasing the pressure drop. In a heat exchanger without baffles the general flow direction would be from the inlet to the outlet and the only contributions to the pressure drop would come from crossing the tube bundle and the friction along the shell wall. Adding baffles disables the flow to go in this direction and therefore pressure drop is increased.

There are several types of baffles. Different baffles are used in different shell configurations and therefore a more detailed explanation is given in the section 3.2.2. But generally baffles can be divided into transverse baffles and longitudinal baffles. In figure 1 the thin vertical lines are transverse baffles as they are orthogonal to the shell. Longitudinal baffles are instead parallel to the shell, see examples of this in figure 2.

3.2.2 Classification

In 1939, an association called TEMA (Tubular Exchanger Manufacturers Association) was founded. TEMA consists of 20 companies and has since the start created standards for shell and tube heat exchangers. The standards developed by TEMA is world leading and are used by most companies that develop and use shell and tube heat exchangers. In this work the TEMA standards are mostly used for the design classification of the shell. In figure 2 the different geometries for the shell types considered in this thesis are defined.

3.2.2.1 Shell type A significant difference between different shell and tube heat exchangers is the shell type. The shell type decides how the fluid flows through the tube bundle and therefore it has a great impact on the heat transfer. The shell type also has a great effect on the shell-side pressure

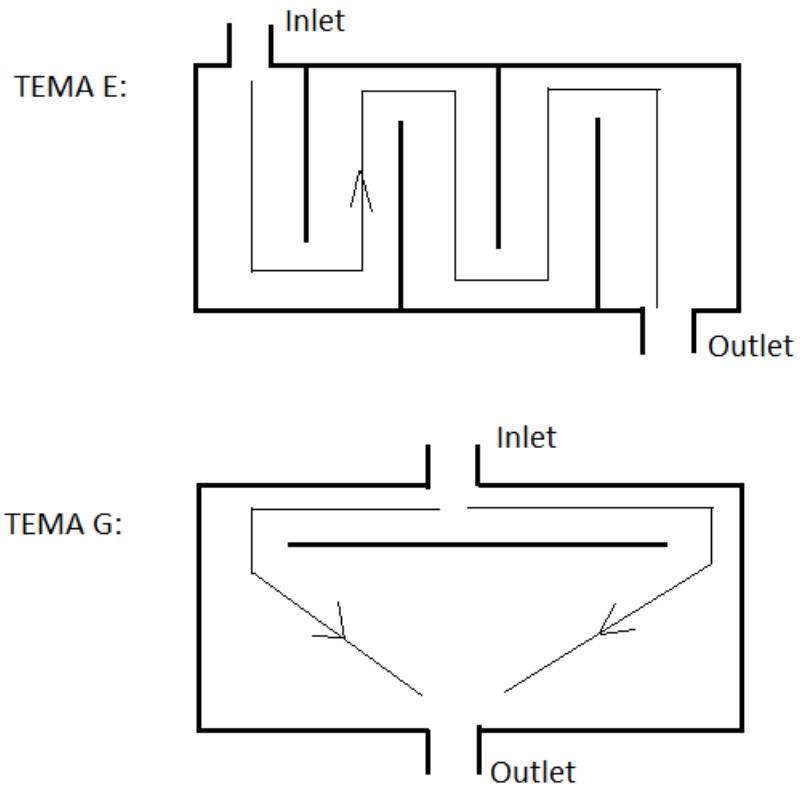

Figure 2: Schematic image of the two shell configurations considered in this thesis with main flow patterns. Classification by TEMA [6]. Flow patterns from [7].

drop. In figure 2 the different shell types that were implemented are listed. The same figure shows the main flow direction in the different shell types. In this master thesis the shell types TEMA E and TEMA G were modelled, below follows a description of those types.

The most common shell type is TEMA E [5]. It has a single shell pass where the fluid is guided by baffles to cross the tube bundle multiple times. The tubes can pass the heat exchanger once or multiple times. TEMA E heat exchanger can be defined more precisely as TEMA $E_{1\text{-}N}$ where N is the number of tube passes. The E shell is mostly used for single-phase application but can also be used for phase-change, both evaporation and condensation. The advantages of using a TEMA E is the relatively simple and cheap design [7].

TEMA G is a split flow heat exchanger where the fluid flows across the shell guided by a longitudinal baffle. This is a more application specific heat exchanger and is mainly used for condensation. With a split flow shell, the pressure drop is essentially the same as in a comparable TEMA E shell but the heat transfer coefficient is higher [7]. In the TEMA G shell vapor enters the shell through an inlet at the top. The vapor is guided by the horizontal, longitudinal baffle to be spread over the entire shell. Flowing downwards the vapor condenses on the cooler, horizontal tubes and the resulting liquid is forced to the bottom of the shell by gravity. At the bottom the liquid is collected and exits the shell through the outlet. The collection of the liquid leads to a liquid level above the bottom. The outlet mass flow rate is dependent on this liquid level.

After this clarification of the different shell types it is obvious that the shell type in figure 1 is TEMA E. For knowledge about other shell types than the two modelled during this thesis please read

[5] and [7].

3.2.2.2 Tube types There are many design choices concerning tubes. Tubes mostly have a circular cross-section but they could also have square or triangular cross-section. In some heat exchanger the tubes are twisted, even though this also is uncommon [5]. To increase heat transfer area, the tubes can be finned on the outside. If finned tubes are chosen the next design question is which type of fins to use. A choice for the tube bundle is the orientation of the tubes, they can be in-lined or staggered. This does not affect the flow inside the tubes but has a great impact on the shell side flow.

3.2.2.3 Flow phase Since a fluid can be either gas or liquid there are four different possible phase configurations. Either the inlet fluid is gas that becomes liquid (condensation), the inlet fluid is liquid that becomes gas (evaporation), the inlet fluid is gas that remains gas throughout the heat exchanger (one-phase) or the inlet fluid is liquid that remains liquids throughout the heat exchanger (one-phase). The two latter are both one-phase flows and are therefore often considered the same phase configuration. That means that there are three phase configurations to consider: one-phase, condensation and evaporation.

3.3 Modelica and Dymola

The modelling in this thesis was done in the modelling language Modelica, in the tool Dymola.

3.3.1 Modelica

Modelica is an open-standard modelling language maintained by the Modelica Association, especially applicable for physical modelling [8]. Special for Modelica compared to other languages is that is equation-based, meaning that commands are written in terms of equations. This is a reason for classifying Modelica as a modelling language instead of a programming language.

$$\begin{cases} Python: & x = -2/3 \\ Modelica: & 3 * x + 2 = 0 \end{cases} \tag{5}$$

Equation 5 shows the difference between an equation-based language and a programming language. Since Modelica is equation-based the equation can be written as it is but in Python the user has to solve the equation in order to find out the value of x. An equation-based language is preferable when dealing with physical modelling for two main reasons. The first reason is that the Modelica user can always write the equation as it is, independent on which quantity that is unknown. The second reason is that some formulas are hard, and some are even impossible, to solve analytically, which the user does not have to do using Modelica.

$$\begin{cases} Python: & \begin{cases} F = m * a \\ m = F/a \\ a = F/m \end{cases} \\ Modelica: & 3 * x + 2 = 0 \end{cases} \tag{6}$$

An example of where the first reason is applicable is shown in equation 6. In Python Newton's second law has to be written in three different ways depending on which of F, m or a that is unknown. In Modelica the equation can be written in one line and it does not matter which quantity that is unknown.

A consequence of the Modelica languages being equation-based is non-causality. It means that the user does not have to know in which order the equations will be solved. Two examples of this is given in figure 7.

$$\begin{cases} Python: & \begin{cases} b = a & a = b * *2 \\ a = 5 & b = a + 1 \end{cases} \\ \\ Modelica: & \begin{cases} b = a & a = b \wedge 2 \\ a = 5 & b = a + 1 \end{cases} \end{cases} \tag{7}$$

In equation 7 the corresponding code is written in Python and Modelica. In the left example Python would not be able to compute b because a would be unknown in the first row. A Modelica compiler could however compute b because it would not matter in which order the statements are placed. The right example shows an implicit system of equations. Again Python would not be able to compute this because b would be unknown in the first row. Modelica could handle this system of equations using an equation solver defined by the simulation environment, for example Dymola.

A more common property of Modelica is that it is object-oriented. Similar to other object-oriented programming languages like Python and Java, Modelica has inheritance which means that one model can inherit the code from another object. This enables code re-usability, the ability that lets two different objects use the same code instead of writing the code in both objects. For more information about the structure of objects in Modelica, please visit reference [8].

A fundamental object in Modelica is the model. A model can represent a physical component such as a pipe or a wall. There are other types of objects than the model. The package type is used as a folder to organize the objects. The record type is an object without any equations, often used to store data. The function type is used as a traditional function, with an algorithm section where commands have to be written in a causal order.

3.3.2 Dymola

Dymola is one of many simulation environments for Modelica [8]. In Dymola the user can write Modelica code or work in a diagram layer. In the latter it is possible to insert models and connect them without writing any code. When the user models in the diagram layer, Modelica code is automatically generated in the code layer. So there are two ways of modelling in Dymola, either writing plain Modelica code or using the diagram layer. An example of the diagram layer is displayed in figure 3. Besides being a user interface, Dymola has a Modelica compiler, manipulates and solves the system of equations and can be used to handle results of simulations.

In Dymola several libraries with pre-programmed models are available for different modelling fields. A fundamental library is the MSL - Modelica Standard Library, that was developed by the Modelica Association. The company where this master thesis was executed, Modelon AB, develops Modelica libraries. Examples of libraries developed by Modelon are the Air Conditioning Library and the Vehicle Dynamics Library [9]. The models in this thesis were based on some models in the Heat Exchanger Library (HXL) and the Modelon Base Library (MBL).

Dymola is a simulation environment but also a compiler that takes the Modelica code and uses it to produce C code which is later compiled to binary machine code.

Dymola has built-in solvers for differential equations. It is possible for the user to choose between these. Examples of solvers in Dymola are Runge-Kutta and Dassl.

3.4 Fluid dynamics theory

3.4.1 Two-phase flow

One main cause of difficulty when dealing with two-phase flow compared to single-phase flow is the variations of flow patterns. Since flow patterns often are important for the computation of pressure drop and heat transfer coefficient this is a major concern with modelling of heat exchangers. In two-phase flow the geometries of the solid in which the fluid travels are also more important in order to

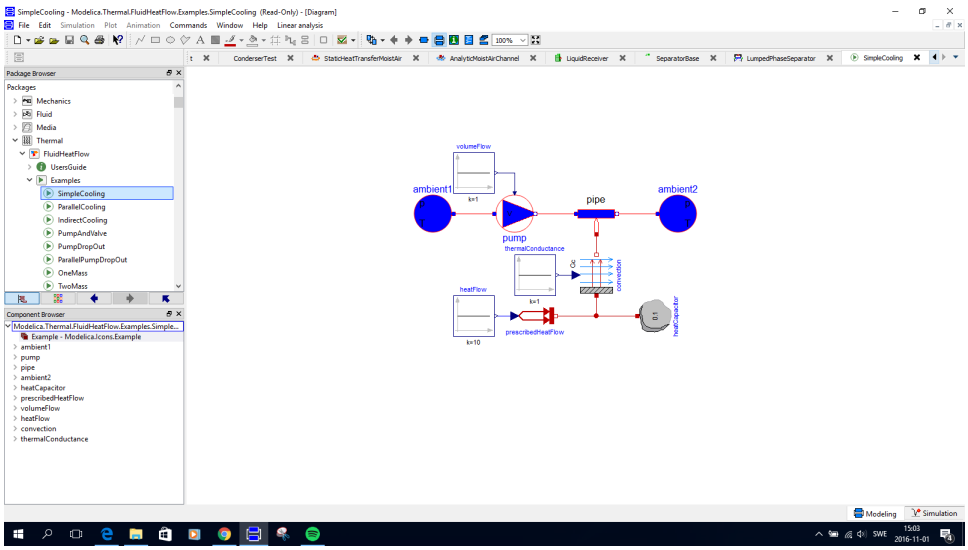

Figure 3: Example of the diagram layer in Dymola. Example was taken from the Modelica Standard Library.

know the dominating flow patterns and thereby calculating pressure drop and heat transfer. Since the geometry of a shell and tube heat exchanger is complex, phase-change causes a lot of difficulty concerning modelling. Below some examples are given to understand the geometry effect on flow patterns.

In figure 4 the main difference between the vertical and the horizontal flow regions is the splitting of the flow. In the horizontal case the vapor is in many cases separated from the liquid due to the large difference in density.

Because of the complexity in calculation of flow properties such as pressure drop, several theories have been developed where a two-phase multiplier can be used according to equation 8 [2].

$$\phi_f^2 = \frac{(dp/dx)_{TF}}{(dp/dx)_f} \tag{8}$$

By using method like this, the procedure of calculating the pressure drop for a two-phase flow is reduced to calculating the pressure drop for the corresponding one-phase flow and multiplying with the two-phase multiplier. Using this kind of method was first introduced in 1949 by Lockhart and Martinelli, who also gave the empirical formula for the two-phase multiplier presented in equation 9 [2].

$$\phi_f^2 = 1 + \frac{C}{X} + \frac{1}{X^2} \tag{9}$$

$$X^2 = \frac{(dp/dx)_f}{(dp/dx)_g} \tag{10}$$

$$C = \begin{cases} 20 & \text{if turbulent flow prevails in the liquid as well as in the gas (tt)} \\ 12 & \text{if the liquid flow is viscous and the gas flow is turbulent (vt)} \\ 10 & \text{if the liquid flow is turbulent and the gas flow is laminar (tv)} \\ 5 & \text{if laminar flow prevails in the liquid as well as in the gas (vv)} \end{cases}$$

Since this theory by Lockhart and Martinelli was published more theories including different equations for the two-phase multiplier have been developed.

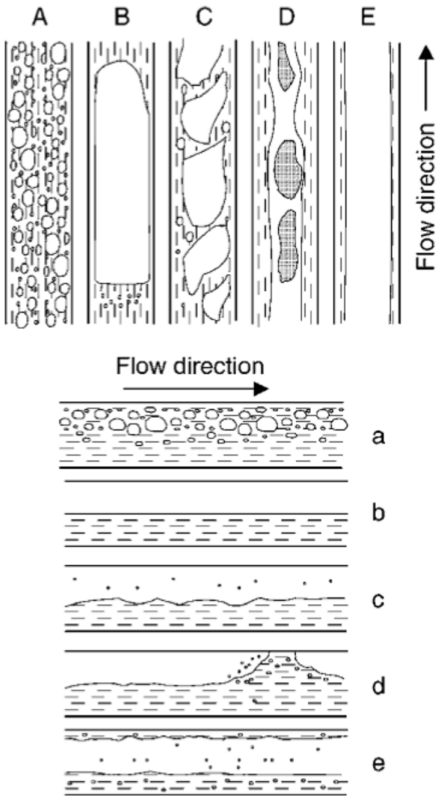

Figure 4: Examples of flow patterns for different two-phase flows in vertical and horizontal geometries respectively, reprinted from reference [10] with permission of the publisher.

As was explained in this section the two-phase flows are hard to generalize and therefore the following chapters were written in order to understand theories developed specifically for shell and tube heat exchangers.

3.4.2 Shell and tube heat exchanger

There are various approaches to modelling of shell and tube heat exchanger. Most of them have been developed since the middle of the 20^{th} century. Since the most common shell type is the TEMA E, most of the methods were developed for this configuration. An early formula for the pressure drop was Kern's method, published in 1950 [11]. Kern's method is displayed in equation 11 and it uses the friction factor from equation 12. Kern's method has been tested against experimental data [7]. At the University of Delaware, a large project was conducted to create a method that would improve the predictions of heat transfer coefficient and pressure drop. When the project was finished in 1963 a report was published including a method called the Delaware method, or sometimes the Bell-Delaware method after Kenneth J. Bell who was one of the leaders of the project [3].

More complicated programs have been developed during the last decades. The organisation HTFS provides a simulation program called TASC and HTRI provides Xchanger Suite. Other than simulation programs like these thermo-fluid simulations are often conducted using CFD (Computational Fluid Dynamics).

3.4.3 Shell side

In this section an overview of the available methods is given. More detailed equations can be found in the section 4 for methods used in the project.

Because of the complex geometry and flow patterns on the shell side, different correlations have to be developed for different configurations. In this project two different shells were considered; TEMA E (one-phase) and TEMA G (condensation). As mentioned in the previous part, TEMA E has been investigated during different projects. One of the first was Kern's method which predicts the pressure drop according to equations 11 and 12 [11]. Compared to later developed methods Kern's method is simple [11]. The equation for the shell side heat transfer coefficient, α_s is also relatively simple, see equation 13 [11].

$$\Delta p_s = 2\frac{f_s G_s^2 D_s (n_b+1)}{D_e \rho_s (\eta_s/\eta_{sw})^{0.14}} \tag{11}$$

$$f_s = \mathbf{0}.4475 Re^{-0.19} \tag{12}$$

$$\alpha_s = \frac{0.36\lambda}{D_e}\left(\frac{D_e G_s}{\eta_s}\right)^{0.55} Pr_s^{1/3}\left(\frac{\eta_s}{\eta_{s,w}}\right)^{0.14} \tag{13}$$

In equation 11 one interesting aspect is the factor $(n_b + 1)$. Since n_b is the number of baffles, $(n_b + 1)$ is the number of cross-flow sections in the heat exchanger. Kern's method assumes that the pressure drop is proportional to the number of cross-flow sections. This assumption will later be compared with the Delaware method.

The Delaware method is much more complicated than Kern's method as it does not assume a perfect design. Instead the Delaware method uses correction factors in order to account for a non-ideal flow [3].

The pressure drop according to the method is displayed in equation 14. R_B, R_L and R_S are the correction factors for the Delaware methods pressure drop correlation. R_B is the correction for bundle bypass flow and is used to account for the fact that the tube bundle does not fill up the entire shell, leaving some space in the shell without tubes. R_L is the correction factor for baffle leakage. In a shell there are spaces between the baffles and the shell. This makes it possible for the fluid to pass through there instead of being forced to go in the main flow direction. In the same way there are spaces between the tubes and the tube holes in the baffles. A part of the fluid could travel that way and that effects the pressure drop. R_S is the correction factor for unequal baffle spacing. The Delaware method assumes that the distance between two adjacent baffles is the same throughout the heat exchanger but the width of the enter and exit sections are not always the same as each other or the cross-flow sections, this is handled by R_S [3].

$$\Delta p_s = (n_b - 1)\Delta p_{ideal} R_B R_L + n_b \Delta p_{w,ideal} R_L + 2\Delta p_{ideal}(1 + N_{cw}/N_c) R_B R_S \tag{14}$$

Equation 14 shows that the pressure drop is divided into three terms. The three terms correspond to the three different sections of the TEMA E heat exchanger in figure 5. The first term calculates the pressure drop for the cross-flow sections, marked with c in figure 5. The second term corresponds to the window sections, marked with w in figure 5. The last term corresponds to the enter and exit sections, marked with e in figure 5. As there are one less cross-flow section than baffles the first term contains the factor $(n_b - 1)$. By the same logic the second term contains the factor n_b (the number of baffles is the same as the number of window sections) and the third term contains a factor 2 (one enter section and one exit section).

The heat transfer coefficient calculated with the Delaware method is displayed in equation 15 [3]. In this equation two additional correction factors are used. J_C is the correction factor for the window section (section w in figure 5). Since the flow in the window section is not cross-flow the heat transfer coefficient is lower, a good shell and tube heat exchanger typically has J_C close to 1 [3]. J_R is the correction factor for laminar flow, for Reynolds number larger than 100, J_R is equal to 1.

$$\alpha_s = \alpha_{ideal} J_C J_B J_L J_R J_S \tag{15}$$

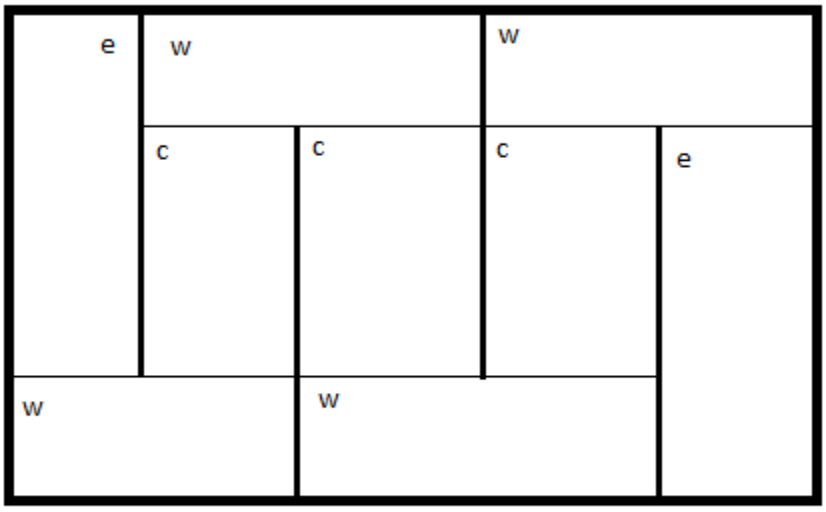

Figure 5: Explanation of sections in a TEMA E shell and tube heat exchanger used in the Delaware method.

The Delaware method above was taken from reference [3]. Other variations of the Delaware method with some differences but with the same structure have been developed. In this project one variant of the Delaware method was taken from reference [10]. To avoid confusion this method was referred to as the modified Delaware method. Note that the intent behind this was not to classify either of the methods as better than the other. The modified Delaware method is presented with different nomenclature than the Delaware method but in this project only the nomenclature from the Delaware method in [3] was used for simplicity. For more details on the Delaware method and the modified Delaware method, see chapter 4.

All methods presented above assume one-phase flow. For correlations on a TEMA E evaporator with evaporation on the shell side a doctoral thesis was conducted by Gavin H. Doo at the University of Strathclyde where the theory and modelling of the tool TASC from the organization HTFS was tested experimentally and the method was improved [12]. As an evaporator is not considered in this project, deeper investigations are left for the interested reader.

The configuration considered besides the TEMA E was the TEMA G condenser. The geometry is much more simple than for the TEMA E but the two-phase flow on the shell side makes it much more complex to model. To estimate the heat transfer of a TEMA G shell, it would be possible to use the method published by McNaught in 1982 that considers condensing on a horizontal tube bundle can be used. Here the heat transfer coefficient is a combination of the gravitational heat transfer coefficient and the shear heat transfer coefficient according to equation 16 [13]. The method presented by McNaught uses the Lockhart-Martinellt two-phase multiplier to calculate the shear heat transfer coefficient from the heat transfer coefficient in the one-phase case.

$$\alpha = (\alpha_{shear}^2 + \alpha_{grav}^2)^{1/2} \tag{16}$$

A similar, but more complicated method was presented by Honda et al., in 1989. The method considers both in-lined and staggered tube layout which makes is good for modelling, since a more generic shell and tube condenser can be achieved. The Nusselt number is displayed in equation 17 [13].

$$Nu = \begin{cases} (Nu_{shear}^4 + (Nu_{grav}Nu_{shear})^2 + Nu_{grav}^4)^{1/4} & \text{if staggered} \\ (Nu_{shear}^4 + Nu_{grav}^4)^{1/4} & \text{if in-lined} \end{cases} \tag{17}$$

3.4.4 Tube side

The tubes naturally have a much simpler geometry which leads to simpler and better correlations for heat transfer coefficients and pressure drops. Some examples of heat transfer correlations are Dittus-Boelter and Gnielinski, presented in equation 18 and 19 respectively. In equation 18 $n = 0.4$ if the tube wall temperature is higher than the fluid temperature and $n = 0.3$ otherwise. Equation 19 uses the friction factor from equation 20 [2]. In equation 18-20 D is the hydraulic diameter which is the diameter for a cylindrical tube [2].

$$Nu_D = 0.023 Re_D^{0.8} Pr^n \tag{18}$$

$$Nu_D = \frac{(f/8)(Re_D - 1000)Pr}{1 + 12.7\sqrt{f/8}(Pr^{2/3} - 1)} \tag{19}$$

$$f = (0.79ln(Re_D) - 1.64)^{-2} \tag{20}$$

For the pressure drop the Moody chart is a well-known tool to calculate the friction factor. Also Haaland's formula could be used for this purpose. Using the friction factor the pressure drop can be calculated using equation 21 [14].

$$\Delta p = f\frac{L}{D}\frac{\rho u^2}{2} \tag{21}$$

Correlations for two-phase flow is also on the tube side geometry dependent, as shown in figure 4. Friedel published in 1979 a method to compute the heat transfer and the pressure drop of a tube with two-phase flow.

4 Modelling

The implementation of Modelica models in the thesis was done in Dymola. In this section the implemented models are presented. The models are based on the MBL and the HXL, some models more than others.

The model for the tube wall uses records for material properties and heat connectors found in the MBL. The rest of the model, including the thermodynamic behavior, was implemented during the thesis.

The model for the tube was almost entirely based on the tube distributed channel model in the MBL. Modifications on the parameters were made in order to make the model easier to use in the implementation of the shell and tube heat exchanger. The Gnielinski method for heat transfer coefficient was added to the model, apart from the models for heat transfer found in the HXL.

The FVM in the TEMA E shell model and the TEMA G shell model was based on the implementation in the channel models in the MBL. The structure of the model, the defining parameters and the correlations for heat transfer and pressure drop were created during the thesis. The receiver used in the TEMA G shell model was inspired from the model for a liquid receiver in the MBL, although many equations were changed.

The models for the shell and tube heat exchanger and the shell and tube condenser were both modelled completely in the thesis. The coupling between the different sub-components as well as the structure of the models was done entirely, although the latter was inspired from other heat exchanger models previously implemented in the HXL. Several sub-components, such as connectors and sources were taken from the HXL and the MBL.

Fluid models in the MBL was used for the fluid properties, such as functions for η and ρ as well as relations between thermodynamic state variables.

4.1 Tube wall

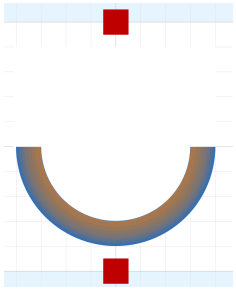

Figure 6: Icon of the tube wall model created in Dymola.

4.1.1 Assumptions

- Cylindrical tubes
- Unfinned tubes
- $L >> D_o - D_i$
- No temperature variation in radial direction
- No heat transfer along the tube wall

In shell and tube heat exchangers, the tubes can have other shapes than cylindrical but that is a less common case. There are also tubes with fins in some heat exchangers but this is also less common

[5]. To include other shapes of tubes or finned tubes would make the model more general but it would require different correlations for heat transfer coefficient and pressure drop on the shell side. The Delaware method assumes unfinned, cylindrical tubes. For tubes in shell and tube heat exchangers the assumption $L >> D_o - D_i$ is valid [2]. This means that the radial temperature variation can be neglected. Since the tubes are long compared to their thickness the temperature of a point in the wall will be more effected by the fluid temperature than the temperature in the rest of the wall.

4.1.2 Design

The $TubeWall$ model inherits from the partial model $GeneralWall$. $GeneralWall$ was designed to be able to be used for many different geometries. This means that models inheriting from $GeneralWall$ must have parameters defining the geometry of the specific model. For $TubeWall$ those parameters are the tube length, L, the inner radius, r_i, and the outer radius, r_o. Geometry parameters are used to calculated the thermal resistance and the mass of the wall. For TubeWall this is done with equation 22 and 23 respectively [2].

$$R_w = \frac{1}{2\pi\lambda L} ln\Big(\frac{r_o}{r_i}\Big) \tag{22}$$

$$m = \rho L \pi (r_o^2 - r_i^2) \tag{23}$$

The tube wall is discretized according to figure 7. The different parts (marked by 1, 2 and 3 in figure 7) each have their own mass, thermal resistance, length and temperature. The reason for doing this will be explained in section 4.4.

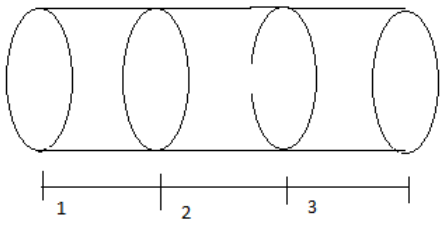

Figure 7: Discretization of the tube wall

The tube wall model consists of two heat flow interfaces, these are the red squares in figure 6. These interfaces are used to model the heat transfer between the wall and the components of each side. Each heat flow interface has a temperature and a heat flow rate. The interfaces are discretized in the same way as the tube wall. This means that each part of the tube wall has its own interfaces and it is thereby possible to connect the different parts of the tube wall to different parts of the tube and the shell. As mentioned before, this is explained in section 4.4.

Since a tube wall consists of metal the tube wall has a metal parameter describing three properties of the metal; thermal conductivity, k, specific heat capacity, c, and density ρ. It is possible for the user to choose a metal with predefined properties but it is also possible to change one or more properties if the user does not agree with the values the are predefined or if the user wants to use a material that is not already implemented.

The use of TubeWall can be different for different users and therefore two Boolean parameters were added. The first one was called $massLessWall$. If $massLessWall$ is true, then the wall cannot store any energy and therefore the sum of the heat flow rates in the interfaces must be equal to zero. If false, the sum of the heat flow rates in the interfaces is the rate of increase of thermal energy in the wall. The second Boolean parameter was called $includeThermalResistance$. If true, the heat flow rate is calculated using equations 25 and 26. If false, the interface temperatures are the same as

the wall temperature. Since a real wall is not mass less and always have some thermal resistance the default values are $massLessWall = false$ and $includeThermalResistance = true$.

4.1.3 Thermodynamics

If the Boolean parameter $massLessWall$ is set to be true the wall cannot hold any energy and therefore the sum of the heat flow rate on the two sides have to be zero, $Q_a + Q_b = 0$. Otherwise the energy balance is calculated by equation 24. Here the subscripts a and b stand for the different interfaces, a is on the inside of the tube wall and b is on the outside. If $includeThermalResistance$ is set to true, equations 25 and 26 are used for the calculation of the heat flow rates. If $includeThermalResistance$ is set to false equation 25 and 26 are replaced by $T_{wall} = T_a = T_b$.

$$mc_p \frac{dT}{dt} = Q_a + Q_b \tag{24}$$

$$Q_a = 2(T_a - T)/R_w \tag{25}$$

$$Q_b = 2(T_b - T)/R_w \tag{26}$$

Dividing the tube wall into parts as in figure 7 means introducing a temperature and interfaces for each part. Since the number of equations and the number of unknowns have to be the same the equations 24-26 have to be calculated for each part.

4.2 Tube

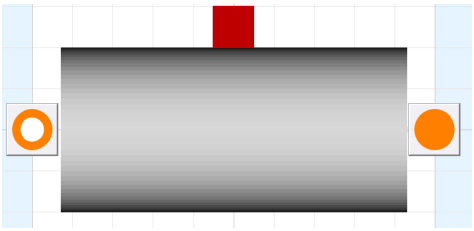

Figure 8: Icon of one of the tube models created in Dymola.

4.2.1 Assumptions

- The fluid is one of the fluids implemented in Modelon Base Library
- Uniform diameter

The implementation of flow channels in MBL and HXL often uses fluid properties defined in fluid models. This means that these models have to be defined with equations for example the thermodynamic state and fluid properties before usage. To assume uniform diameter is not very limiting since this is very common amongst shell and tube heat exchangers.

4.2.2 Design

One main idea of the thermo-fluid modelling in the Heat Exchanger Library (HXL) is the control volume (CV). This means that the tube was discretized in several CV's in the main flow direction, much like the tube wall discretization in figure 7. Each CV is treated as uniform part of the tube. This means that the entire CV has the same fluid properties (for example temperature and pressure). This modelling method is called the finite volume method (FVM). The number of CV's, $n_{orthogonal}$, is user defined.

Besides $n_{orthogonal}$, the tube is defined be the inner diameter D, the length $Length$, the heat transfer area A_{heat}, the number of parallel channel $n_{channel}$, and the medium. As mentioned in the assumptions, the diameter can be assumed to be the same for the entire tube. Therefore, the diameter is a scalar. Length is not a scalar but a vector where the i^{th} element describes the length of the i^{th} CV. The same way of modelling was done for the heat transfer area. To read about an advantage of this, see section 4.4. The medium model is used to calculated the fluid properties. The parameter $n_{channel}$ can be used to model several tubes that can be assumed to be exactly the same. This way the number of unknowns and the number of equations can be reduced, read more in section 4.4 and 4.6.

An important modelling term is the thermodynamic state. The state is a way to describe the properties of the fluid. The state is defined by the two state variables (assuming pure fluid). The idea behind state variables is that they should be enough to describe the fluid properties completely. One example that is often used for single-phase flow is pressure together with temperature. If the pressure and temperature of the fluid is known, the thermodynamic state can be uniquely defined (assuming single-phase). Pressure and temperature are not always suitable for describing the fluid. This can be visualized by water being heated beyond the boiling point. At the moment the water begins to boil the temperature is 100^oC (assuming atmospheric pressure). During boiling the energy of the water rises but the temperature remains the same until the phase-change is complete and temperature starts to rise again. This shows that the temperature does not describe the fluid well during a phase-change. For two-phase flows, pressure and enthalpy is a better choice as state variable as they describe the fluid properties uniquely. In the Modelon Base Library (MBL), which HXL is based on, different fluids are implemented. Each of them have equations for fluid properties such as density and viscosity where the only input variable is the state. These equations were used in the tube models.

As described above the tube is divided into control volumes. Each CV has its own state and therefore its own fluid properties. Each control volume can also be connected to an external heat flow interface, represented by the red square in figure 8. The energy increase of the i^{th} control volume is therefore calculated as the difference between the energy coming from the $(i-1)^{th}$ control volume and the energy flowing in to the $(i+1)^{th}$ control volume plus the heat flow coming from the heat connector. In the first control volume the energy coming from the inlet interface, represented as the orange circle to the left in figure 8, is used instead of a previous control volume. The inlet interface is, when used, connected to a flow source defining the boundary condition. The corresponding technique is used for the last control volume.

Two different tube models were implemented, one for single-phase flow and one for two-phase flow. This was done partly because different models for heat transfer and pressure drop exists for single-phase flow and two-phase flow.

4.2.3 Heat transfer

For the calculation of the heat transfer coefficient in the single-phase case two different correlations are available; Dittus-Boelter and Gnielinski. Both methods are presented in section 3.4.4. For two-phase tubes several correlations exist. All of them are re-used from previous models in HXL. Different methods for condensation and evaporation are available. For condensation the method developed by Shah ([15]) is the main method, but since this method is known to be better for high mass fluxes the method developed by Akers, Deans and Crosser ([16]) is given as an alternative at lower mass fluxes than $200 kg/sm^2$ [17]. For evaporation methods by Kandlikar ([18]), Gungor and Winterton ([19]) and Chen ([20]) are available. These methods have been compared and the recommended correlation is the one developed by Kandlikar [21]. As these methods were not implemented during this thesis the equations are not given and the interested reader is recommended to look in the references for more details.

In both the single-phase and two-phase tube model, the user can choose a heat transfer model called ConstantCoefficient in order to decide the heat transfer coefficient without any pre-programmed methods.

4.2.4 Pressure drop

In each control volume a pressure drop has to be calculated. This is done by using a pressure drop correlation. The user can choose if the pressure drop should be calculated from the mass flow or reverse. Therefore, the different models usually have correlations for the two alternatives.

For the single-phase tube model the default model for pressure drop is *DetailedWallFriction*. Assuming the pressure drop is calculated from the mass flow and not reverse the correlation is presented in equations 27-30. Note that equation 29 is not complete. If $Re_1 < Re < 4000$ interpolation is used to compute f. Here D is the hydraulic diameter and ϵ is the roughness factor. Other correlations are available for the user but since all of them were implemented before this thesis only the default correlation is presented.

$$Re = \frac{4\dot{m}}{4D\eta} \tag{27}$$

$$Re_1 = \begin{cases} 745e^1 & \text{if } \epsilon/D \leq 0.0065 \\ 745e^{0.0065D/\epsilon} & \text{if } \epsilon/D > 0.0065 \end{cases} \tag{28}$$

$$f = \begin{cases} \frac{64}{Re} & \text{if } Re < Re_1 \\ 0.25\left(\frac{Re}{log\left(\frac{\epsilon}{3.7D} + \frac{5.74}{Re^{0.9}}\right)}\right)^2 & \text{if } Re > 4000 \end{cases} \tag{29}$$

$$\Delta p = \frac{L\eta^2}{2\rho D^3} f \tag{30}$$

For the two-phase case the default correlation is the method developed by Friedel ([22]). The method is complex and the equations can be found in the reference. The method was experimentally tested to agree well for evaporation [23] and condensation [24].

4.3 TEMA E shell

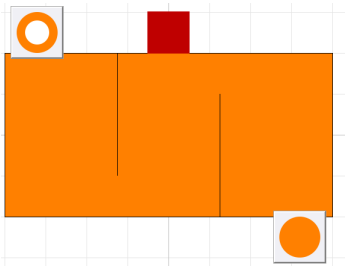

Figure 9: Icon of the TEMA E shell model created in Dymola.

4.3.1 Assumptions

- TEMA E shell type
- Single-segmental baffles
- Limited baffle cut, $0.15 < B_c < 0.45$
- In-lined (90^o) or staggered (30^o) tube layout
- Equally distanced baffles

- Unfinned tubes

The idea behind assuming one special kind of shell in the model is that the flow patterns are significantly different for different shell types and therefore different models for pressure drop and heat transfer would be required. Both versions of the Delaware method used for the modelling assume single-segmental baffles. There are several different kinds of baffles that are used in shell and tube heat exchangers, but the single-segmental baffle is one of the most common. The two most common of them are shown in figure 10 [5].

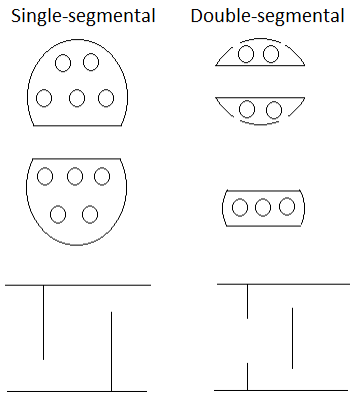

Figure 10: Schematic picture of the two most common baffle types. The first two pictures in each column are the different parts of the baffle configuration seen from the cross-sectional view of the shell. The pictures at the bottom are how the different parts are located relative to each other in the heat exchanger.

The Delaware method also assumes a limited range of the baffle cut. The baffle cut is defined as the fraction of the shell diameter not covered by the baffle. The assumed range can be considered practical [3]. The tube layout has an impact on the pressure drop and the heat transfer in the shell by effecting the flow pattern. In the Delaware method, 45^o is also considered but only 90^o and 30^o were implemented since they are most common [3, 10]. The two tube layouts are visualized in figure 11.

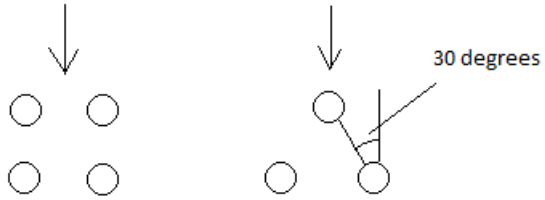

Figure 11: Picture of the two tube layouts considered in the modelling. In-lined to the left and staggered to the right. The arrows represent the main flow direction

Both the Delaware method and the modified Delaware method assume equal distance between the baffles. It would not be hard to change this assumption in the shell model but the gain from doing so would be small considering the fact that it is unusual to have different distances between the baffles.

As mentioned in section 3, the Delaware method assumes unfinned tubes. For finned tubes the heat transfer and pressure drop will change and other correlations are needed.

4.3.2 Design

The implementation of the shell model is similar to the implementation of the tube model. The fluid travels through control volumes with a thermodynamic state defining the properties of the fluid. Each control volume can be connected to a heat port to impose heat transfer and the energy increase of a control volume is calculated as the difference between the energy coming in to the control volume from the previous CV and the energy flowing to the next CV plus the heat from the heat connector. Just like the tube model, the shell model has sub-models for the calculation of heat transfer coefficient and pressure drop. For more details on this kind of implementation, which is standard in HXL, see section 4.2.

The major difference between the shell model and the tube model is the calculation of heat transfer coefficients and pressure drop together with the geometrical parameters. The control volumes in the shell model are designed according to figure 12. The discretization in figure 12 corresponds to the different sections in figure 5. Therefore, the pressure drop is calculated differently in the different sections (see section 4.3.4).

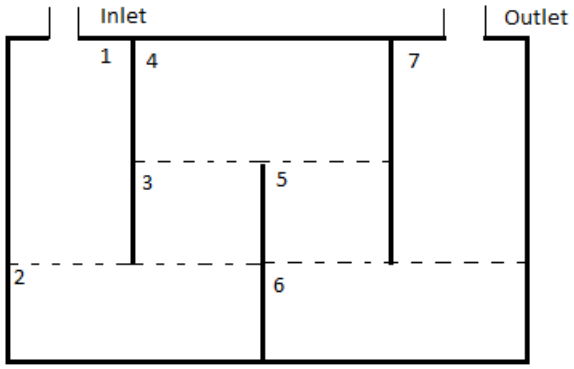

Figure 12: Discretization of the TEMA E shell model. The discretization corresponds to the different sections in figure 5

The defining parameters are listed below. Some of them are also presented in figures 13-14. Besides these parameters, the tube layout and the medium are important for the modelling of the shell.

- D_s : Shell diameter
- B : Baffle distance
- B_{in} : Width of the enter section
- B_{out} : Width of the end section
- B_c : Baffle cut (fraction of shell diameter)
- δ_{sb} : Shell-to-baffle distance
- δ_{tb} : Tube-to-baffle distance
- P_T : Tube pitch, orthogonal to the main flow direction
- P_L : Tube pitch, parallel to the main flow direction
- n_b : Number of baffles
- N_{ss} : Number of sealing strip pairs

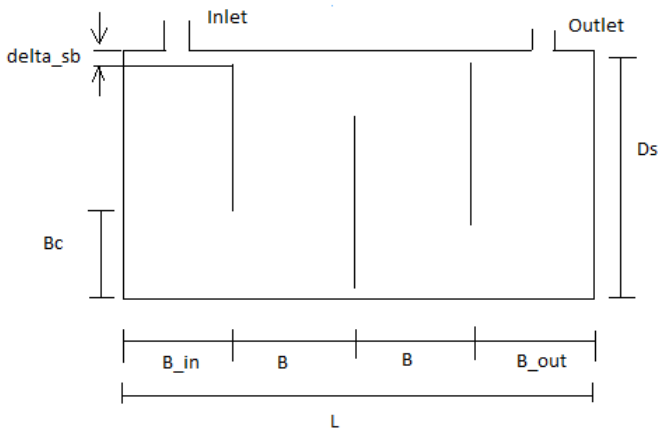

Figure 13: Definition of geometrical parameters for the shell model

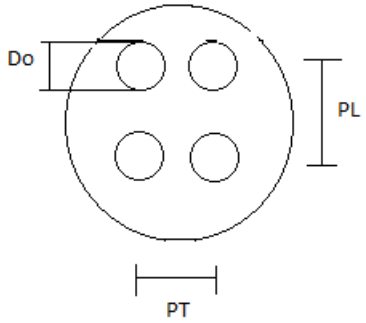

Figure 14: Definition of geometrical parameters for the shell model concerning the tube bundle

- D_{otl} : Outer tube limit diameter
- n_t : Total number of tubes in the heat exchanger
- n_w : Number of tubes in one window section
- D_o : Outer tube diameter
- Tube layout : In-lined or staggered

4.3.3 Heat transfer

Two methods for the computation of the shell side heat transfer coefficient were implemented; The Delaware method and the modified Delaware method. The reason for using both correlations was to compare the results and investigate if any of the methods is better then the other. Both have a large set of equations and are fairly complicated. However, almost all equations are explicit. The equations given are sufficient to implement the methods but most of the derivation are left out. For this derivation and more background knowledge, see [3] for the Delaware method and [10] for the modified Delaware method. In the following sections each of the methods are described. Some equations have different expressions for different ranges of a variable, for example Re. In the implementation these equations are not written with if-statements but instead splice functions have been used in order to

obtain numerical stability and to shorten the simulation time. The splice function is visualized in figure 15.

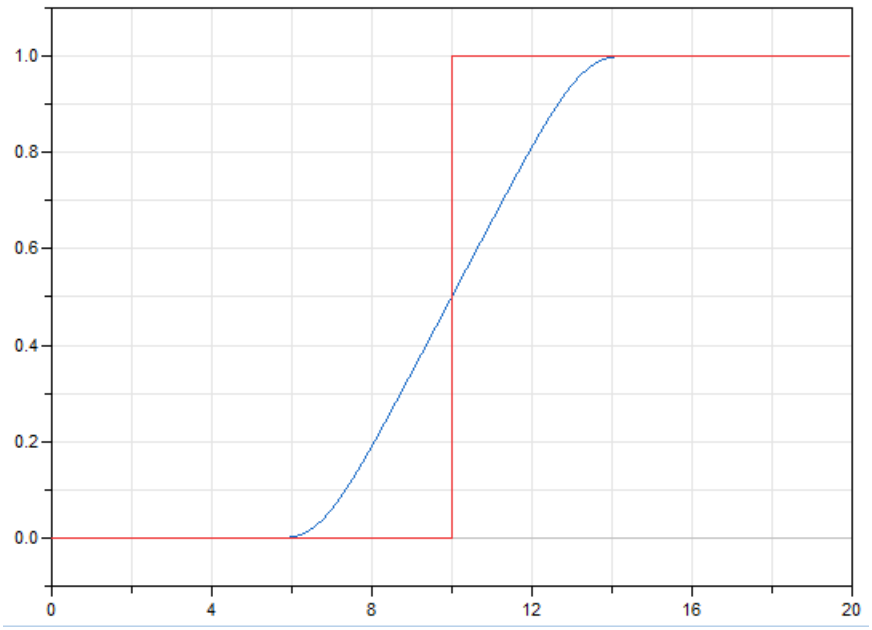

Figure 15: Visualization of the smoothing used in the implementation. The step-function uses an if-statement and the smooth function uses a splice function.

4.3.3.1 Delaware method As previously presented in equation 15 the heat transfer coefficient can be determined as below. The expression for α_s is a product of an idealized heat transfer coefficient, calculated in equation 32, and a set of correction factors. The corrections factors were introduced in section 3 and the equations for them will be presented in this section.

$$\alpha_s = \alpha_{ideal} J_C J_B J_L J_R J_S \tag{31}$$

$$\alpha_{ideal} = \frac{j c_p \dot{m}}{S_m Pr^{2/3}} \tag{32}$$

α_{ideal} is calculated from the Colburn j-factor, presented in equation 34. Equation 34 on its hand builds in equation 35 and j and a are calculated from four coefficients a_{1-4}, which are results of analysis of experimental data. These are presented in equations 36-39. S_m in equation 34 is the cross-flow area displayed in equation 33.

$$S_m = B\left(D_s - D_{otl} + \frac{D_{otl} - D_o}{P_T}(P_T - D_o)\right) \tag{33}$$

$$j = a_1 \left(\frac{1.33}{PT/D_o}\right)^a Re^{a_2} \tag{34}$$

$$a = \frac{a_3}{1 + 0.14 Re^{a_4}} \tag{35}$$

$$a_1 = \begin{cases} \text{In-lined:} & \begin{cases} 0.97 & \text{if } Re < 10 \\ 0.9 & \text{if } 10 < Re < 100 \\ 0.408 & \text{if } 100 < Re < 1000 \\ 0.107 & \text{if } 1000 < Re < 10000 \\ 0.37 & \text{if } 10000 < Re \end{cases} \\ \text{Staggered:} & \begin{cases} 1.4 & \text{if } Re < 10 \\ 1.36 & \text{if } 10 < Re < 100 \\ 0.593 & \text{if } 100 < Re < 1000 \\ 0.321 & \text{if } 1000 < Re < 10000 \\ 0.321 & \text{if } 10000 < Re \end{cases} \end{cases} \tag{36}$$

$$a_2 = \begin{cases} \text{In-lined:} & \begin{cases} -0.667 & \text{if } Re < 10 \\ -0.631 & \text{if } 10 < Re < 100 \\ -0.46 & \text{if } 100 < Re < 1000 \\ -0.266 & \text{if } 1000 < Re < 10000 \\ -0.395 & \text{if } 10000 < Re \end{cases} \\ \text{Staggered:} & \begin{cases} -0.667 & \text{if } Re < 10 \\ -0.657 & \text{if } 10 < Re < 100 \\ -0.477 & \text{if } 100 < Re < 1000 \\ -0.388 & \text{if } 1000 < Re < 10000 \\ -0.388 & \text{if } 10000 < Re \end{cases} \end{cases} \tag{37}$$

$$a_3 = \begin{cases} 1.187 & \text{if in-lined} \\ 1.45 & \text{if staggered} \end{cases} \tag{38}$$

$$a_4 = \begin{cases} 0.37 & \text{if in-lined} \\ 0.519 & \text{if staggered} \end{cases} \tag{39}$$

The correction factor for the window section (see section w in figure 5), J_C, is presented in equation 40. It depends only on F_c, the fraction of the tubes in cross flow section (see section c in figure 5). F_c is calculated using equation 41 and depends on θ_{ctl} from equation 42 which depends on the center tube limit diameter in equation 43.

$$J_C = 0.55 + 0.72F_c \tag{40}$$

$$F_c = 1 + \frac{sin(\theta_{ctl}) - \theta_{ctl}}{\pi} \tag{41}$$

$$cos\left(\frac{\theta_{ctl}}{2}\right) = \frac{D_s(1 - 2B_c)}{D_{ctl}} \tag{42}$$

$$D_{ctl} = D_{otl} - D_o \tag{43}$$

The second correction factor, J_L, is for baffle leakage and is displayed in equation 44. It depends on the two area ratios r_l and r_s calculated in equation 45 and 46 respectively. The areas S_{sb} and S_{tb} can be determined from the equations 47-49.

$$J_L = 0.44(1 - r_s) + (1 - 0.44(1 - r_s))e^{-2.2r_l} \tag{44}$$

$$r_l = \frac{S_{sb} + S_{tb}}{S_m} \tag{45}$$

$$r_s = \frac{S_{sb}}{S_{sb} + S_{tb}} \tag{46}$$

$$S_{sb} = D_s \delta_{sb} (\pi - \theta_{ds}/2) \tag{47}$$

$$\theta_{ds} = 2arccos(1 - 2B_c) \tag{48}$$

$$S_{tb} = 0.5\pi D_o \delta_{tb} n_t (1 + F_c) \tag{49}$$

The third correction factor, J_B, is for tube bundle bypass flow and is presented in equation 50. It depends on the ratio between the sealing strips (N_{ss}) and the number of tube rows in cross-flow section, N_c (from equation 52, r_{ss} (equation 51), the experimentally derived parameter C_J (see equation 54) and the areas S_m and S_b. The latter is displayed in equation 55.

$$J_B = \begin{cases} 1 & \text{if } r_{ss} \geq 0.5 \\ e^{-C_J S_b / S_m (1 - (2r_{ss})^{1/3})} & \text{if } r_{ss} < 0.5 \end{cases} \tag{50}$$

$$r_{ss} = \frac{N_{ss}}{N_c} \tag{51}$$

$$N_c = \frac{D_s(1 - 2B_c)}{P'_T} \tag{52}$$

$$P'_T = \begin{cases} P_T & \text{if in-lined} \\ P_T \sqrt{3}/2 & \text{if staggered} \end{cases} \tag{53}$$

$$C_J = \begin{cases} 1.35 & \text{if } Re < 100 \\ 1.25 & \text{if } Re \geq 100 \end{cases} \tag{54}$$

$$S_b = B(D_s - D_{otl}) \tag{55}$$

The fourth correction factor account for the unequal baffle spacing in the enter section and in the end section (see section e in figure 5). It uses the coefficient n_1 from equation 57.

$$J_S = \frac{n_b - 1 + (B_{in}/B)^{1-n_1} + (B_{out}/B)^{1-n_1}}{n_b - 1 + B_{in}/B + B_{out}/B} \tag{56}$$

$$n_1 = \begin{cases} 1/3 & \text{if } Re < 100 \\ 0.6 & \text{if } Re \geq 100 \end{cases} \tag{57}$$

The fifth, and last, correction factor is for the laminar flow. J_R is displayed in equation 58 and depends on the N_{ct} from equation 59. N_{ct} on its hand depends on n_b, N_c and N_{cw}. The latter is the number of tube rows in the window section and is presented in equation 60. However, the equation 58 is incomplete. In the case $20 < Re < 100$ the correction factor is calculated as an interpolation between the two values.

$$J_R = \begin{cases} 1 & \text{if } Re \geq 100 \\ (10/N_{ct})^{0.18} & \text{if } Re \leq 20 \end{cases} \tag{58}$$

$$N_{ct} = (n_b + 1)(N_c + N_{cw}) \tag{59}$$

$$N_{cw} = \frac{0.8 B_c D_s}{P'_T} \tag{60}$$

4.3.3.2 Modified Delaware method The modified Delaware method taken from reference [10] uses several correction factor to compute the Nusselt number for the shell, Nu_{shell}, see equation 62. This can be used to calculate the heat transfer coefficient using equation 61. The steps to compute the shell side Nusselt number will be given in this section, including equations for the correction factors.

$$\alpha = \frac{\lambda Nu_{shell}}{\pi D_o/2} \tag{61}$$

$$Nu_{shell} = f_W Nu_{bundle} \tag{62}$$

The Nusselt number for flow on the outside of a tube bundle, Nu_{bundle}, is displayed in equation 63. The correction factor, f_P, is used for the changes in the fluid properties in the thermal boundary layer and is given in equation 64. n_p in the same equation depends on the type of gas. For more information, see [10].

$$Nu_{bundle} = f_P Nu_{0,bundle} \tag{63}$$

$$f_P = \begin{cases} \text{For liquids:} & \begin{cases} \left(\frac{Pr}{Pr_w}\right)^{0.25} & \text{if } \frac{Pr}{Pr_w} > 1 \\ \left(\frac{Pr}{Pr_w}\right)^{0.11} & \text{if } \frac{Pr}{Pr_w} < 1 \end{cases} \\ \text{For gases:} & \left(\frac{T_m}{T_w}\right)^{n_p} \end{cases} \tag{64}$$

The ideal Nusselt number for a tube bundle, $Nu_{0,bundle}$, is given in equation 65. It is the product of the correction factor f_A, used to account for different tube layouts and $Nu_{l,0}$, a combination of the laminar and the turbulent Nusselt number.

$$Nu_{0,bundle} = f_A Nu_{l,0} \tag{65}$$

$$Nu_{l,0} = 0.3 + \sqrt{Nu_{l,lam}^2 + Nu_{l,turb}^2} \tag{66}$$

$$Nu_{l,lam} = 0.664\sqrt{Re_{\psi,l}}Pr^{1/3} \tag{67}$$

$$Nu_{l,turb} = \frac{0.037 Re_{\psi,l}^{0.8} Pr}{1 + 2.443 Re_{\psi,l}^{-0.1}(Pr^{2/3} - 1)} \tag{68}$$

Equations 67-68 use a special Reynold's number, given in equation 69. Here the coefficient ψ is used. ψ depends on the ratios between the transverse and longitudinal tube pitch and is shown in equation 70. The tube pitch ratios, a and b, are displayed in equations 71-72.

$$Re_{\psi,l} = \frac{\dot{m}\pi D_o}{2\psi D_s B \eta} \tag{69}$$

$$\psi = \begin{cases} 1 - \frac{\pi}{4a} & \text{if } b \geq 1 \\ 1 - \frac{\pi}{4ab} & \text{if } b < 1 \end{cases} \tag{70}$$

$$a = \frac{P_T}{D_o} \tag{71}$$

$$b = \frac{P_L}{D_o} \tag{72}$$

The tube arrangement factor, f_A, also depends on ψ and the tube pitch ratios. It can be calculated using equation 73.

$$f_A = \begin{cases} 1 + \frac{0.7(b/a-0.3)}{\psi^{1.5}(b/a+0.7)^2} & \text{if in-lined} \\ 1 + \frac{2}{3b} & \text{if staggered} \end{cases} \tag{73}$$

The correction factor f_W from equation 62 is given as the product of three other factors, see equation 74.

$$f_W = f_G f_L f_B \tag{74}$$

The first of the correction factors contributing to f_W is f_G, shown in equation 75. R_G is the ratio between the number of tubes in the window section (see section w in figure 5) and the total number of tubes in the heat exchanger and it is given in equation 76.

$$f_G = 1 - R_G + 0.524 R_G^{0.32} \tag{75}$$

$$R_G = \frac{n_w}{n_t} \tag{76}$$

The second correction factor in equation 74 is f_L. It is used for the leakage between through the baffles. Equations for S_{sb} and S_{tb} are given in section 4.3.3.1 and R_Q is defined through equations 78-80, where N_t is the number of tube rows in the heat exchanger.

$$f_L = 0.4 \frac{S_{tb}}{S_{tb} + S_{sb}} + \left(1 - 0.4 \frac{S_{tb}}{S_{sb} + S_{tb}}\right) e^{-1.5 R_Q} \tag{77}$$

$$R_Q = \frac{S_{sb} + S_{tb}}{B L_e} \tag{78}$$

$$L_e = 2\delta_s b + N_t e \tag{79}$$

$$e = \begin{cases} \text{In-lined:} & P_T - D_o \\ \text{Staggered:} & \begin{cases} \sqrt{\left(\frac{P_T}{2}\right)^2 + P_L^2} - D_o & \text{if } b < 0.5\sqrt{2a+1} \\ P_T - D_o & \text{if } b \geq 0.5\sqrt{2a+1} \end{cases} \end{cases} \tag{80}$$

The third, and last, correction factor in equation 74 is f_B. It is used to account for tube bundle bypass flow and is displayed in equation 81. β is given in equation 82, R_B is given in equation 83 and the area it depends on, A_b, is given in equation 84. r_{ss} is presented in section 4.3.3.1.

$$f_B = \begin{cases} e^{-\beta R_B \left(1 - (2r_{ss})^{1/3}\right)} & \text{if } r_{ss} \leq 1/2 \\ 1 & \text{if } r_{ss} > 1/2 \end{cases} \tag{81}$$

$$\beta = \begin{cases} 1.5 & \text{if } Re_{\psi,l} < 100 \\ 1.35 & \text{if } Re_{\psi,l} \geq 100 \end{cases} \tag{82}$$

$$R_B = \frac{A_b}{S_e} \tag{83}$$

$$A_b = \begin{cases} B(\delta_{sb} - e) & \text{if } e < \delta_{sb} \\ 0 & \text{if } e \geq \delta_{sb} \end{cases} \tag{84}$$

4.3.4 Pressure drop

The same methods used for the heat transfer coefficient are used for the pressure drop correlation. Just like for the heat transfer, these methods include a large set of equations involving many geometrical calculations. Smoothing of discontinuous equations was done in the same fashion as for heat transfer, see figure 15.

4.3.4.1 Delaware method Recall the equation for the shell side pressure drop presented in equation 14:

$$\Delta p_s = (n_b - 1)\Delta p_{ideal} R_B R_L + n_b \Delta p_{w,ideal} R_L + 2\Delta p_{ideal}(1 + N_{cw}/N_c) R_B R_S \tag{85}$$

As for the heat transfer correlation Δp is calculated as a combination of ideal pressure drops and correction factors. The idealized pressure drop for the cross-flow section (see section c in figure 5), Δp_{ideal}, is displayed in equation 86. In a similar fashion to the heat transfer correlation the idealized pressure drop depends on the idealized friction factor, f_{ideal}, from equation 87. f_{ideal} depends on a set of experimentally derived coefficients, b and b_{1-4}, presented in equations 88-92. The geometrical coefficients N_c and S_m are explained in section 4.3.3.1. The rest of the components in equation 85 are displayed in this section.

$$\Delta p_{ideal} = \frac{2 f_{ideal} N_c \dot{m}^2}{\rho S_m^2} \tag{86}$$

$$f_{ideal} = b_1 \left(\frac{1.33}{PT/D_o} \right)^b Re^{b_2} \tag{87}$$

$$b = \frac{b_3}{1 + 0.14 Re^{b_4}} \tag{88}$$

$$b_1 = \begin{cases} \text{In-lined:} & \begin{cases} 35 & \text{if } Re < 10 \\ 32.1 & \text{if } 10 < Re < 100 \\ 6.09 & \text{if } 100 < Re < 1000 \\ 0.0815 & \text{if } 1000 < Re < 10000 \\ 0.391 & \text{if } 10000 < Re \end{cases} \\ \text{Staggered:} & \begin{cases} 48 & \text{if } Re < 10 \\ 45.1 & \text{if } 10 < Re < 100 \\ 4.57 & \text{if } 100 < Re < 1000 \\ 0.486 & \text{if } 1000 < Re < 10000 \\ 0.372 & \text{if } 10000 < Re \end{cases} \end{cases} \tag{89}$$

$$b_2 = \begin{cases} \text{In-lined:} & \begin{cases} -1 & \text{if } Re < 10 \\ -0.963 & \text{if } 10 < Re < 100 \\ -0.602 & \text{if } 100 < Re < 1000 \\ -0.22 & \text{if } 1000 < Re < 10000 \\ -0.148 & \text{if } 10000 < Re \end{cases} \\ \text{Staggered:} & \begin{cases} -1 & \text{if } Re < 10 \\ -0.973 & \text{if } 10 < Re < 100 \\ -0.476 & \text{if } 100 < Re < 1000 \\ -0.152 & \text{if } 1000 < Re < 10000 \\ -0.123 & \text{if } 10000 < Re \end{cases} \end{cases} \tag{90}$$

$$b_3 = \begin{cases} 6.3 & \text{if in-lined} \\ 7 & \text{if staggered} \end{cases} \tag{91}$$

$$b_4 = \begin{cases} 0.378 & \text{if in-lined} \\ 0.5 & \text{if staggered} \end{cases} \tag{92}$$

The idealized pressure drop in the window section, $\Delta p_{w,ideal}$, is presented in equation 93. N_{cw}, θ_{ds}, F_c and S_m are presented in section 4.3.3.1 and the window flow area,S_w, is given in equation 94. The fraction of the tubes in the window section, F_w, used in equation 94 is displayed in equation 95.

$$\Delta p_{w,ideal} = \frac{(2 + 0.6N_{cw})\dot{m}^2}{2\rho S_m S_w} \tag{93}$$

$$S_w = D_s^2(\theta_{ds} - sin(\theta_d s))/8 - n_t F_w \pi D_o^2/4 \tag{94}$$

$$F_w = \frac{1 - F_c}{2} \tag{95}$$

The first correction factor, R_L is for baffle leakage and it is given in equation 96. The area ratios r_l and r_s are presented in section 4.3.3.1 and p is given in equation 97.

$$R_L = e^{-1.33(1+r_s)r_l^p} \tag{96}$$

$$p = 0.8 - 0.15(1 + r_s) \tag{97}$$

The second correction factor is for tube bundle bypass flow and it is displayed in equation 98. The areas S_m and S_b as well as r_{ss} are given in section 4.3.3.1. C_R is presented in equation 99.

$$R_B = \begin{cases} 1 & \text{if } r_{ss} \geq 0.5 \\ e^{-C_R S_b/S_m(1-(2r_{ss})^{1/3})} & \text{if } r_{ss} < 0.5 \end{cases} \tag{98}$$

$$C_R = \begin{cases} 4.5 & \text{if } Re < 100 \\ 3.7 & \text{if } Re \geq 100 \end{cases} \tag{99}$$

The third, and last, correction factor for the shell side pressure drop is R_S. It accounts for the effect of unequal baffle spacing in the enter section and in the end section and is presented in equation 100. The coefficient n_2 is given in equation 101.

$$R_S = \frac{(B/B_{in})^{2-n_2} + (B/B_{out})^{2-n_2}}{2} \tag{100}$$

$$n_2 = \begin{cases} 1 & \text{if } Re < 100 \\ 0.2 & \text{if } Re \geq 100 \end{cases} \tag{101}$$

4.3.4.2 Modified Delaware method Much like the Delaware method the pressure drop is calculated in different ways for the different sections in figure 5, see equation 102.

$$\Delta p = (n_b - 1)\Delta p_c + 2\Delta p_e + n_b \Delta p_w \tag{102}$$

The pressure drop in the cross-flow section is given in equation 103, where Δp_c is the ideal pressure drop displayed in equation 104. f_L is the correction factor for the baffle leakage and is presented in equation 105. r_s and R_Q in this equation are given in sections 4.3.3.1 and 4.3.3.2 respectively while p is given in section 4.3.4.1. f_B is the correction factor for tube bundle bypass flow, see equation 106.

It is identical to equation 81 but β is computed differently, see equation 107. The ε in equation 104 is a friction factor and is given by a set of equations, see equations 108-117.

$$\Delta p_c = f_L f_B \Delta p_c \tag{103}$$

$$\Delta p_{c,0} = \varepsilon N_c \frac{\dot{m}^2}{2\rho S_m^2} \tag{104}$$

$$f_L = e^{-1.33(1+r_s)R_Q^p} \tag{105}$$

$$f_B = \begin{cases} e^{-\beta R_B\left(1-(2r_{ss})^{1/3}\right)} & \text{if } r_{ss} \leq 1/2 \\ 1 & \text{if } r_{ss} > 1/2 \end{cases} \tag{106}$$

$$\beta = \begin{cases} 3.7 & \text{if } Re < 100 \\ 4.5 & \text{if } Re \geq 100 \end{cases} \tag{107}$$

$$\varepsilon = \begin{cases} \varepsilon_{lam} f_{z,l} + \varepsilon_{turb} f_{z,t}\left(1 - e^{-\frac{Re+1000}{2000}}\right) & \text{if in-lined} \\ \varepsilon_{lam} f_{z,l} + \varepsilon_{turb} f_{z,t}\left(1 - e^{-\frac{Re+200}{1000}}\right) & \text{if staggered} \end{cases} \tag{108}$$

$$\varepsilon_{lam} = \begin{cases} \frac{f_{a,l,f}}{Re} & \text{if in-lined} \\ \frac{f_{a,l,v}}{Re} & \text{if staggered} \end{cases} \tag{109}$$

$$\varepsilon_{turb} = \begin{cases} \frac{f_{a,t,f}}{Re^{0.1b/a}} & \text{if in-lined} \\ \frac{f_{a,t,v}}{Re^{0.25}} & \text{if staggered} \end{cases} \tag{110}$$

$$f_{a,l,f} = \frac{280\pi\left(\left(\sqrt{b} - 0.6\right)^2 + 0.75\right)}{(4ab - \pi)a^{1.6}} \tag{111}$$

$$f_{a,t,f} = \left(0.22 + 1.2\frac{(1 - 0.94/b)^{0.6}}{(a - 0.85)^{1.3}}\right)10^{0.47(b/a-1.5)} + 0.03(a-1)(b-1) \tag{112}$$

$$f_{a,l,v} = \begin{cases} \frac{280\pi\left((\sqrt{b}-0.6)^2+0.75\right)}{(4ab-\pi)a^{1.6}} & \text{if } b \geq 0.5\sqrt{2a+1} \\ \frac{280\pi\left((\sqrt{b}-0.6)^2+0.75\right)}{(4ab-\pi)c^{1.6}} & \text{if } b < 0.5\sqrt{2a+1} \end{cases} \tag{113}$$

$$f_{a,t,v} = 2.5 + \left(\frac{1.2}{(a - 0.85)^{1.08}}\right) + 0.4\Big(b/a - 1\Big)^3 - 0.01\Big(a/b - 1\Big)^3 \tag{114}$$

$$f_{z,l} = \left(\frac{\eta_w}{\eta}\right)^{\frac{0.57}{(Re(4ab/\pi-1))^{0.25}}} \tag{115}$$

$$f_{z,t} = \left(\frac{\eta_w}{\eta}\right)^{0.14} \tag{116}$$

$$c = \sqrt{\left(\frac{a}{2}\right)^2 + b^2} \tag{117}$$

The pressure drop in the window sections is given as a combination of the laminar pressure drop, $\Delta p_{w,lam}$, the turbulent pressure drop, $\Delta p_{w,turb}$ and two correction factors, f_Z and f_L, see equation

118. The laminar and the turbulent pressure drops can be calculated by a set of equation, see equations 119-121. S_m, N_{cw}, F_c and $\theta_d s$ are given in section 4.3.3.1 and S_w is given in section 4.3.4.1. f_Z can be determined from equation 122.

$$\Delta p_w = \sqrt{\Delta p_{w,lam}^2 + \Delta p_{w,lam}^2} f_Z f_L \tag{118}$$

$$\Delta p_{w,lam} = \frac{\dot{m}^2}{2\rho S_m^2}\left(\frac{56 N_{cw}}{\frac{\dot{m}e}{\rho S_m \eta}} + \frac{52}{\frac{D_w \dot{m}}{\rho S_m \eta}}\frac{B}{Dw} + 2\right) \tag{119}$$

$$\Delta p_{w,turb} = (0.6 N_{cw} + 2)\frac{\dot{m}^2}{2\rho S_m^2} \tag{120}$$

$$D_w = \frac{4 S_w}{\pi D_o n_t (1 - F_c)/2 + D_s \theta_d s} \tag{121}$$

$$f_Z = \begin{cases} f_{z,l} & \text{if } Re < 100 \\ f_{z,t} & \text{if } Re \geq 100 \end{cases} \tag{122}$$

The pressure drop in the enter and end sections can be computed with equation 123.

$$\Delta p_{e,0} = f_B \Delta p_{c,0}\left(\frac{N_{cw}}{N_c}\right)\left(\frac{B}{B_e}\right)^{2-m} \tag{123}$$

In equation 123, B_e stands for B_{in} in the enter section and B_{out} in the end section. The coefficient m can be taken from equation 124.

$$m = \begin{cases} 0.1 b/a & \text{if in-lined} \\ 0.25 & \text{if staggered} \end{cases} \tag{124}$$

4.4 Shell and tube heat exchanger

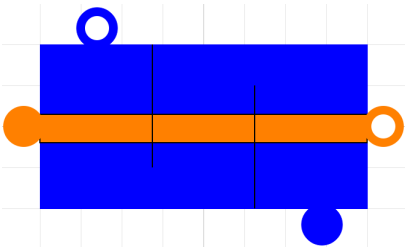

Figure 16: Icon of one of the shell and tube heat exchanger models created in Dymola. This example has liquid on the shell side and gas on the tube side.

4.4.1 Assumptions

- TEMA E shell
- Heads and nozzles excluded
- Single-phase flow on the shell side
- All tubes have the same geometry, inlet- and outlet conditions and initial values
- Pressure drop and heat transfer in bends are neglected

- Bends in multi-pass heat exchangers are outside of the shell

The model is a TEMA E shell and tube heat exchanger. The reason for implementing only one configuration in the model is, as was mentioned for the shell model, that other configurations require different correlations for heat transfer and pressure drop. But also the coupling between the shell and the tubes would be different for another type of shell and tube heat exchanger.

The reasons for excluding heads and nozzles is the complexity this would imply for the implementation of the model and the lack of correlations for the fluid dynamics in these components.

In this thesis two heat exchangers were implemented. One TEMA E shell and tube heat exchanger for single-phase flow and one TEMA G shell and tube condenser for two-phase flow. There are TEMA E heat exchangers with other phase configurations than single-phase but those were not considered in the thesis [12].

The reason to assume that all tubes have the same geometry is partly because this is assumed by the Delaware but also that some tubes should be identical. The latter is also the reason to assume that all tubes have the same inlet- and outlet conditions and the same initial values. Since the flow in the tubes come from a head and ends in another head it is not wrong to assume that the inlet- and outlet conditions are the same. The initial values could be different but because of the shared front-end head and rear-end head this is not likely.

The assumptions concerning bends are discussed in section 4.4.2.

4.4.2 Design

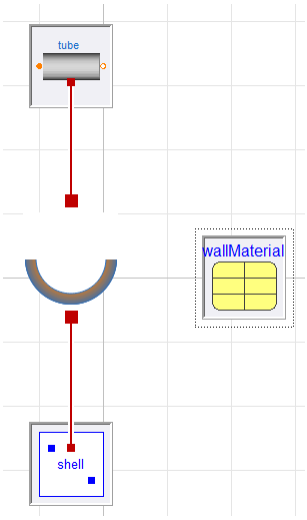

Figure 17: Graphical view of the template model for the TEMA E shell and tube heat exchanger. The component on the top symbolized the tubes, the components in the middle symbolizes the tube wall and the component in the bottom is the shell. The object to the right is the record for the wall material. The red lines represent heat transfer connections.

A physical shell and tube heat exchanger is built on a shell and tubes with a tube wall separating the tube side from the shell side. To mimic the reality as much as possible this was also done in Modelica, see figure 17. But the heat transfer connections between the three components are not trivial and have to be motivated. Heat transfer connection means that heat can flow between the components and the heat flow rate is calculated according to $Q = \alpha A(T_1 - T_2)$, where Q is the heat flow rate from the component with temperature T_1 to the component with temperature T_2. If Q is positive component 2 is heated and component 1 is cooled, if Q is negative the opposite occurs.

The first modelling question that arises is how many tubes that should be implemented. The trivial idea is naturally to implement all tubes, but this leads to heavy calculations since the number

of tubes easily can be a few hundred. But recalling the discretization of the shell model in figure 12 it is possible to realize that some tubes would be identical, see figure 18 were the heat exchanger is divided into three horizontal regions. Every tube in a given region is connected to the same control volumes of the shell as the others in the same region. Since the temperature is the same in an entire control volume, this mean that the heat transferred to two different tubes in the same region must be the same. By assuming that all tubes have the same geometry, the same inlet- and outlet boundary conditions and the same initial values the conclusion is that two tubes in the same region must be identical. If two tubes are known to be identical, there is of course no need to simulate them both. Instead are tubes in a single region represented by one tube. Here the parameter $n_{channel}$ (explained in section 4.2) was used. If the number of tubes in the top region of the heat exchanger is 100 then the tube connected to the top part would have $n_{channel} = 100$. Since every tube have a tube wall, the same modelling design was used for the tube wall.

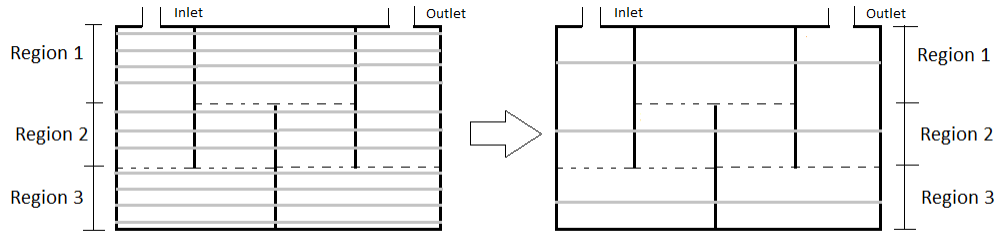

Figure 18: Schematic visualization of the simplification of the tubes and the connections to the shell.

When the idea of connection was done the second modelling issue was the discretization, which already has been done for the shell side. The tubes are discretized with $n_b + 1$ CV's (n_b is the number of baffles), see figure 19. In the same figure the connection between the tubes and the shell is visualized in detail depending on flow arrangement (co-current or counter-current). As shown in figure 17 the tube was connected to the tube wall that was connected to the shell. This means that the couplings shown in figure 19 are actually the couplings between the tube wall and the shell. For a simple implementation the tubes and the tube walls are always connected parallel to each other and they always have the same discretization. This means that the numbers in the different control volumes in the tubes in figure 19 are the same for the tube wall. Note that careful consideration must be made if the number of baffles is even instead of odd as in figure 19. Then the shell side outlet would be on the downside instead of the upside.

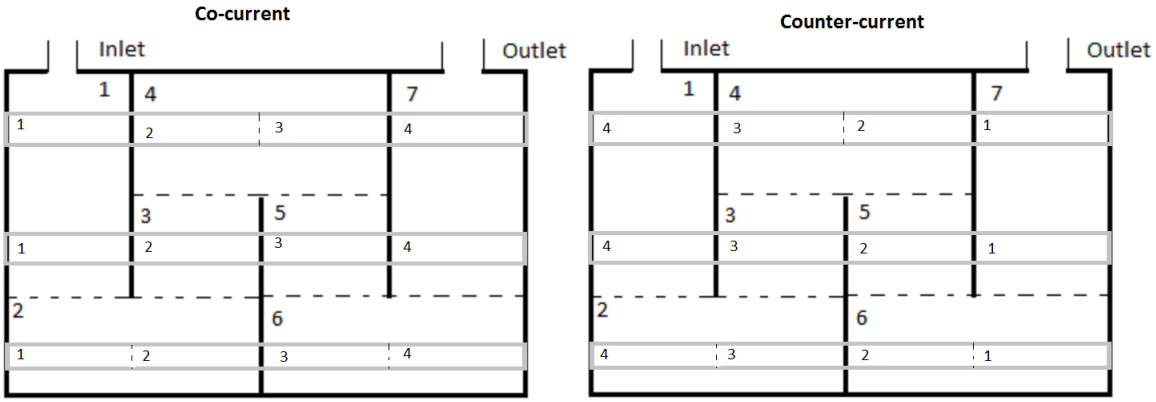

Figure 19: Schematic visualization of the connection between the tube/tube wall and the shell. Note the difference in connection depending on the flow arrangement.

The arrangements in figures 18 and 19 assume that the number of tube passes is one ($NTP = 1$). Since the intention was to have a model that did not make this assumption another connection must be implemented for heat exchanger with $NTP > 1$. The idea behind the connection between the tube wall and the shell for a multi-pass shell and tube heat exchanger is shown in figure 20. In the multi-pass heat exchanger, the tubes are divided into two groups, instead of three as in the single-pass heat exchanger. The first group passes through the upper region on its first pass. The second group passes through the middle region on its first pass. The rest of the connections are dependent on NTP and therefore they are visualized in figure 20. In the actual implementation of the tubes for the multi-pass heat exchanger not only two tubes were implemented. Instead each tube pass has two tubes, resulting in $2NTP$ tubes in total. All these tubes are shown in figure 20. The tubes are connected to each other and the connection are visualized as the grey half-circles in figure 20. Note that this connection is not a heat connection, the purpose of this connection is for the fluid that travels out of one tube to continue in to the next. This is done be connecting the flow ports, see the circles in figure 8.

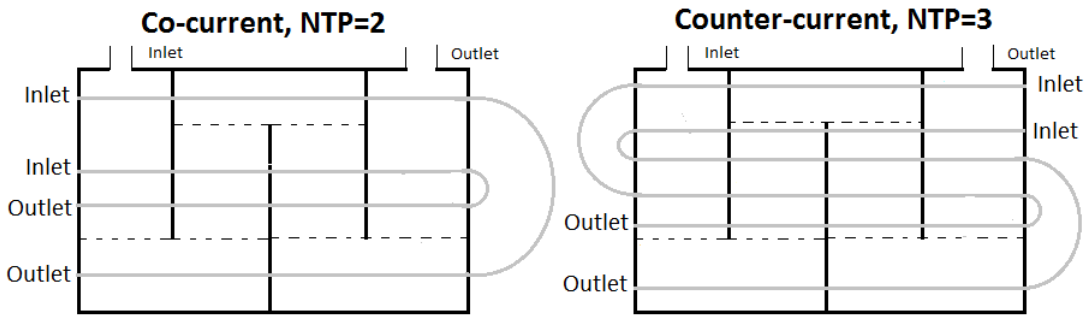

Figure 20: Connections between the tube wall and the shell for two examples of a multi-pass heat exchanger.

This implementation requires some assumptions. Since only the first tube is in the upper region and only the last tube is in the lower region, the model assumes that no fluid travels through tubes in the upper or lower region twice. The model also assumes the path of the tubes. For example, the tubes that starts in the middle region ends in the lower region for a heat exchanger with $NTP = 3$, see the right part of figure 20. Because of the symmetry in a heat exchanger with $NTP = 2$ these assumptions cannot be any problem. Since the baffle cut is the same in the entire heat exchanger, the tubes in the upper region on the first pass should be the tubes in the lower region on the second pass while the rest travel both passes in the middle region. The first assumption should not be a problem for a heat exchanger with small baffle cuts. But if the NTP or B_c is high this could be a problem. For example, a shell and tube heat exchanger with $NTP = 100$ would naturally have tubes with several passes in the upper region. But for heat exchangers with reasonable NTP and B_c the modelling should be valid. As shown in figure 20, the bends are outside of the shell. It is not given that this is the case for all shell and tube heat exchangers but to have the bends inside the shell would affect the flow pattern on the shell side in a manner that could not be handled by the Delaware method. An assumption implied by this modelling idea is that the pressure drop through the bends are neglected. This will affect all multi-pass shell and tube heat exchangers and it is wrong. The reason for doing this was simplicity. The fluid is also immune to heat losses (or gains) through the bend. This will likely contribute to errors in the simulations because there is always something surrounding the tubes that can transfer heat. But to reduce losses in a real heat exchanger this effect would be minimized which is an argument for not including it in the model.

In figure 17, the template for the shell and tube heat exchanger is presented. The full model requires more components and an example of this is shown in figure 21. Besides the components in figure 17 this model has a split (object in the upper-right part of the figure), a join (object in the upper-left part of the figure), two inlets, two outlets and a summary record. The split divides the flow equally between the tubes (only the inlet tubes for a multi-pass heat exchanger) and the join collects

the flow from the tubes (only the outlet tubes for a multi-pass heat exchanger). The inlet ports can be used to connect the heat exchanger to flow sources and the outlet ports can be used to connect the heat exchanger to sinks. The flow sources and the sinks determine the boundary conditions. The summary record can be used when simulating to have easy access to variables of the heat exchanger. But it is not only new components that separates the template model in figure 17 from the full model in figure 21. The template model has partial tube model while the full model must specify if the tube should have single-phase flow or two-phase flow. As mentioned in section 4.2 two tube models were created, one for single-phase flow and one for two-phase. To implement a full heat exchanger model requires to choose one of the two.

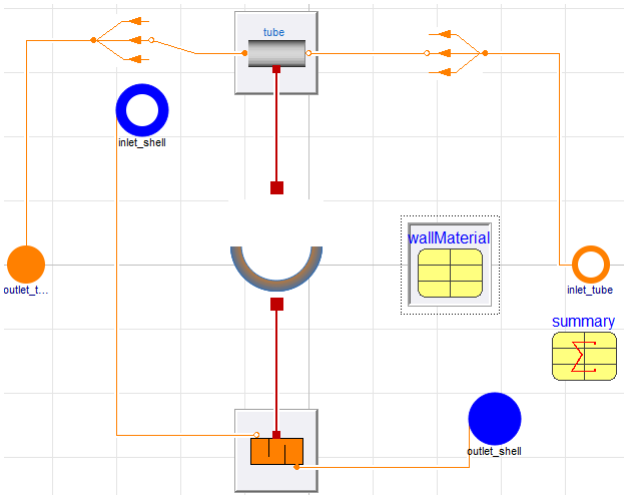

Figure 21: Graphical layer of one of the shell and tube heat exchanger model. This example has liquid on the shell side and gas on the tube side.

To model a specific shell and tube heat exchanger parameter for geometry, initial values and correlations for the sub-components are available. Also the tube medium, the shell medium and the tube wall material can be chosen. Apart from the parameters for the sub-components the user may also choose the flow arrangement (counter-current or co-current) and whether to have two-phase flow in the tubes. As mentioned above, boundary conditions such as temperature, mass flow rate and pressure are chosen with flow sources and sinks.

4.5 TEMA G shell

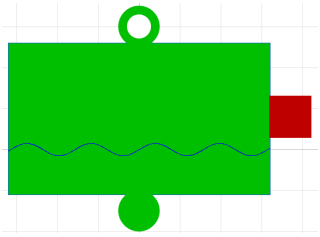

Figure 22: Icon of the TEMA G shell model created in Dymola.

4.5.1 Assumptions

- One outlet for both liquid and gas

- Equal flow over the entire length of the shell
- Same geometry for all tubes

The reason for implementing only one outlet is simplicity. To have more outlets would require knowledge about how these outlets are placed and more boundary conditions would be needed. The implemented model therefore works best for full condensation, which means that all the fluid leaving the condenser through the outlet is liquid. As shown in figure 2 as real TEMA G shell has a longitudinal baffle in order to divide the fluid over the length of the heat exchanger. In this model that baffle is replaced by the assumption that the fluid is equally divided over the length. The assumption of equal geometry for all tubes is to make the implementation of the pressure drop and heat transfer models easier.

4.5.2 Design

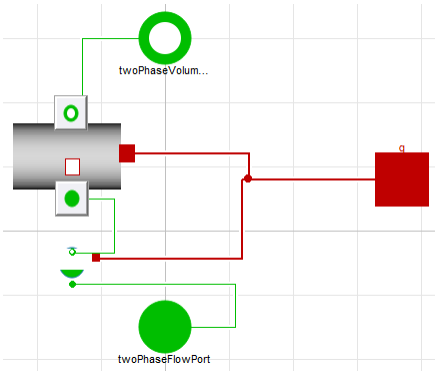

Figure 23: Diagram layer of the TEMA G shell implemented in Modelica.

In figure 23 the diagram layer of the TEMA G shell model is displayed. The circular object at the top is the inlet. From the inlet the fluid travels to the condenser pipe, shown as the rectangle in the middle of figure 23. After passing through the condenser pipe the fluid continues to the shell receiver before exiting from the outlet port in the bottom.

The condenser pipe was constructed much like a tube, with control volumes, thermodynamic states, a heat transfer model and a friction model. The number of control volume in the condenser pipe is the same as the number of tube rows in the heat exchanger. The receiver was built with only one control volume, but it also has a heat transfer model and thermodynamic states. Even though the receiver only has one control volume it has the same number of heat flow ports as the condenser pipe, in order to be able to add them.

The condenser pipe in designed to handle the heat transfer for the two-phase flow, which means the fluid above the liquid level. The heat transfer for the fluid below the liquid level is handled by the receiver. This means that the total heat flow rate from the shell is calculated as the sum of the heat flow rate from the condenser pipe and the heat flow rate from the receiver. This is illustrated as the red connection lines in figure 23. If a tube row is below the liquid level the corresponding heat flow rate in the condenser pipe is zero. And if a tube row is above the liquid level the corresponding heat flow rate is zero. This means that in the event that the liquid level rises above a tube row it is required that the heat flow rate in the condenser pipe is set to zero and in the receiver it needs to be calculated from a version of equation 1 instead of being zero. Naturally the reverse would happen if the liquid level sinks below a tube row. For numerical stability it is important that this action is not done discontinuously. Therefore, a splice function is used to smooth the transition between the two states.

The purpose of the receiver is not only to transfer heat to the tubes. The main purpose of the receiver is to calculate the liquid level and depending on this liquid level calculate the quality of the

outgoing flow. By knowing the thermodynamic state of the fluid in the receiver the vapor quality, x, and the density, ρ, may be calculated. Using this together with the total volume of the shell (which is known from the geometrical parameters) the liquid volume (the volume covered by the liquid) can be calculated. From the liquid volume the liquid level can be calculated implicitly using equation 125 where V_{liq} is the liquid volume, L is the shell length and R is the shell radius.

$$V_{liq} = L\left((level - R)\sqrt{2R \cdot level - level^2} + R^2 arcsin\left(\frac{level - R}{R}\right) - R^2 arcsin(-1)\right) \tag{125}$$

Note that the liquid level is computed using the fluid properties in the receiver but it is used also for the condenser pipe, which may have other fluid properties. If no very rapid changes are expected in the heat exchanger this modelling method should be valid.

The shell can be defined by the following parameters:

- D_s : Shell diameter
- L : Shell length
- P_T : Tube pitch, orthogonal to the main flow direction
- P_L : Tube pitch, parallel to the main flow direction
- n_{tubes} : Number of tubes in each row (see more in section 4.6)
- D_o : Outer tube diameter
- A_{in} : Cross-sectional area at the first tube row
- Tube layout : In-lined or staggered

4.5.3 Heat transfer

The heat transfer coefficient is calculated differently for the condenser pipe and the receiver. Since the receiver only has liquid under the liquid level α can be computed using a version of the Delaware method, presented in section 4.3.3.1. But in the condenser pipe the flow is condensing and the heat transfer coefficient has to be calculated accordingly. The method developed by Honda can be used for condensation on a tube bundle with downwards flow, which is the case for the TEMA G condenser.

4.5.3.1 Honda The Honda method computes the Nusselt number which is related to the heat transfer coefficient according to equation 126.

$$\alpha = \frac{Nu\lambda_{liq}}{\pi D_o/2} \tag{126}$$

The Honda method calculates the Nusselt number as a combination of the gravitational Nusselt and the shear Nusselt number dependent on the tube layout, see equation 127.

$$Nu = \left\{(Nu_{grav}^4 + Nu_{shear}^4)^{1/4} \right. \tag{127}$$

The two different Nusselt numbers can be computed using a set of different Reynold's numbers, see equations 128-133. Several of these equations depend on the heat flux, q. Since the heat flux is heat flow rate per unit area and that the heat flow rate depends on the heat transfer coefficient the Honda method is implicit. Furthermore, the fluid properties are declared below:

- ρ_{liq} : Liquid density
- ρ_{vap} : Vapor density

- η_{liq} : Liquid dynamic viscosity
- η_{vap} : Vapor dynamic viscosity

$$Nu_{shear} = \begin{cases} 0.053\left(Re_{vap}^{-0.2} + 18\left(\frac{q_n}{i_{fg}\rho_{vap}u_n}\right)^{1/2}\right)\left(\frac{\rho_{vap}}{\rho_{liq}}\right)^{1/2}\frac{Re_{liq}Pr_{liq}^{0.4}}{Re_{shear}^{0.2}} & \text{if in-lined} \\ 0.165\left(\frac{P_T}{P_L}\right)^{0.7}\left(Re_{vap}^{-0.4} + 1.83\left(\frac{q_n}{i_{fg}\rho_{vap}u_n}\right)\right)^{1/2}\left(\frac{\rho_{vap}}{\rho_{liq}}\right)Re_{liq}Pr_{liq}^{0.4} & \text{if staggered} \end{cases} \tag{128}$$

$$Nu_{grav} = Gr^{1/3}\left((1.2Re_{grav}^{-0.3})^4 + (0.072Re_{grav}^{0.2})^4\right)^{1/4} \tag{129}$$

$$Re_{grav} = \begin{cases} \text{In-lined:} & 2\pi D_o \sum_{j=1}^{n} \frac{q_j}{\eta_{liq} i_{fg}} \\ \text{Staggered:} & \begin{cases} 2\pi D_o \sum_{j=1}^{(n+1)/2} \frac{q_{2j-1}}{\eta_{liq} i_{fg}} & \text{if n odd} \\ 2\pi D_o \sum_{j=1}^{n-1} \frac{q_{2j}}{\eta_{vap} i_{fg}} & \text{if n even} \end{cases} \end{cases} \tag{130}$$

$$Re_{shear} = \begin{cases} Re_{grav} & \text{if } n = 1 \\ 2\pi D_o \frac{q_n + \sum_{j=1}^{n-1} \frac{q_j D_o}{P_T}}{\eta_{liq} i_{fg}} & \text{if } n > 1 \end{cases} \tag{131}$$

$$Re_{liq} = \frac{\rho_{liq} u_n D_o}{\eta_{liq}} \tag{132}$$

$$Re_{vap} = \frac{\rho_{vap} u_n D_o}{\eta_{vap}} \tag{133}$$

u_n in equations 128-133 is the vapor velocity and can be determined by equation 134. Gr in equation 129 is the Grashof number and it is given in equation 135.

$$u_n = \begin{cases} \left(\frac{P_T}{P_T - D_o}\right)\left(\frac{\dot{m}}{A_{in}\rho_{vap}}\right) & \text{if } n = 1 \\ \frac{\frac{\dot{m}P_T}{A_{in}} - \pi D_o \sum_{j=1}^{n-1} \frac{q_j}{i_{fg}}}{\rho_{vap}(P_T - D_o)} & \text{if } n > 1 \end{cases} \tag{134}$$

$$Gr = g\left(\frac{\rho_{liq} - \rho_{vap}}{\rho_{liq}}\right)\left(\frac{\rho_{liq}^2 D_o^3}{\eta_{liq}^2}\right) \tag{135}$$

4.5.4 Pressure drop

The pressure drop is calculated as a combination of the Chisholm correction factor and the Delaware method, see equation 136. Chisholm's two-phase correction factor is displayed in equations 137-138 [10].

$$\Delta p_{TP} = \phi \Delta p_{liq} \tag{136}$$

$$\phi = 1 + \left(\Gamma^2 - 1\right)\left(\frac{21x^{0.9}(1 - x^{0.9})x^{1.8}}{\Gamma}\right) \tag{137}$$

$$\Gamma = \sqrt{\frac{\rho_{liq}}{\rho_{vap}}}\left(\frac{\eta_{vap}}{\eta_{liq}}\right)^{0.1} \tag{138}$$

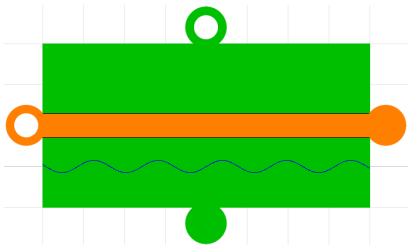

Figure 24: Icon of one of the shell and tube heat exchanger models created in Dymola. This example has gas on the tube side.

4.6 Shell and tube condenser

4.6.1 Assumptions

- TEMA G shell
- The shell side fluid condenses
- All tubes in one tube row are equally heated
- Initial conditions, boundary conditions and geometrical parameters are equal for all tubes
- The shell side fluid is equally divided over the length of the condenser

The geometry of the heat exchanger is important for the shell side flow patterns which effect the pressure drop and the heat transfer. Therefore, it is necessary to implement only one shell configuration in each model. The phase configuration (condensation, evaporation or single-phase) is also necessary to define since the heat transfer model depends on this, at least the method of Honda which was used in the shell model. The Honda method calculates the heat transfer coefficient for every tube row, the heat transfer coefficient of one tube row depends on how many tube rows that are above. This is one reason to assume that all tubes in one tube row are equal. More reasons will be given in section 4.6.2. As shown in figure 2, the tube side of shell and tube heat exchanger begin in a front-end head and end in a rear-end head. This is why it is reasonable to assume that the boundary conditions are the same for all tubes. The geometry of different tubes is not necessary the same in theory but for the simplicity of implementation, both for the shell and tube condenser and for the heat transfer and pressure drop correlations, the geometrical parameters were assumed to be identical for all tubes. Figure 2 show that a TEMA G shell and tube condenser has a longitudinal baffle in order to split the flow over the length of the heat exchanger. In the model no such baffle was implemented. Instead the fluid is assumed to be divided equally.

4.6.2 Design

The main components of a shell and tube condenser is the shell, the tubes and the tube wall between the shell and the tubes. Therefore, the implementation in Modelica was done in a similar fashion, see figure 25. But the implementation is more complex than what is shown in figure 25.

As for the single-phase shell and tube heat exchanger the first choice to make in order to model is how many tubes that should be implemented. For both the single-phase heat exchanger and the condenser it would be very time consuming to simulate a model with all actual tubes implemented since the equation system would be very large. For the TEMA E shell and tube heat exchanger some tubes were assumed to have equal heat transfer with the shell. This idea could be reused for the condenser model. Since the heat transfer correlation of Honda calculates the heat transfer coefficient for every tube row it would be logical to discretize the shell according to the tube rows, see the left side of figure 26. Because of this shell side discretization, the knowledge that the temperature is the

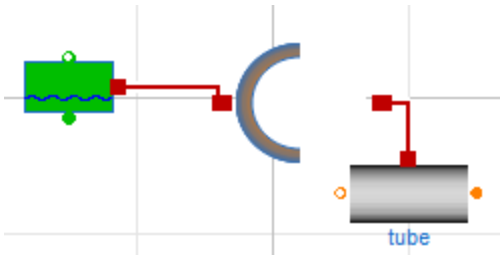

Figure 25: Diagram layer of the template for the shell and tube condenser models. The object to the left is the shell, the object in the middle is the tube wall and the object to the right is the tubes. The red line symbolizes the heat transfer connections. The model also has a record defining the wall material but this was left out to focus on the most important components.

same in an entire control volume and the assumption that the tubes are identical the tube side can be simplified according to figure 26. This mean that one tube per tube row was used to symbolize the entire tube row. This simplification was done using the parameter $n_{channel}$ in the tube wall and tube model. But to know the value of $n_{channel}$ the number of tubes in each tube row must be known. This is defined by the parameter n_{tubes}. As an example the number of tubes in the shell and tube condenser in figure 26 is defined by $n_{tubes} = [2, 4, 4, 2]$. Since a tube is only connected to one control volume of the shell, the tubes are discretized with one control volume.

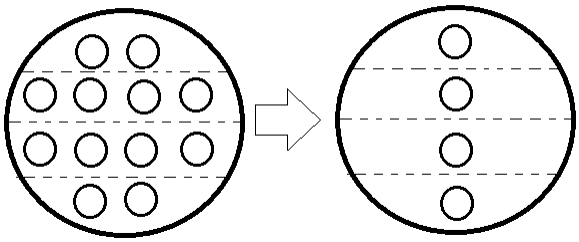

Figure 26: The left side of the figure describes the shell side discretization of the shell and tube condenser. The right side of the picture shows the simplification of the tubes in the condenser model.

The discretization of the shell gives a rather simple way to extend the model to handle multi-pass condensers, see figure 27. The number of control volumes on the shell side are simply multiplied by the number of tube passes, compared to a single-pass condenser. In the same way the number of implemented tubes are multiplied by the number of tube passes, compared to the single-pass case. The tubes are then connected to each other as shown in figure 27.

In the template model in figure 25, only the main components of the shell and tube condenser are defined. Based on this template model two full shell and tube condenser models were implemented. One with liquid on the tube side and one with gas on the tube side, the latter is shown in figure 28. Added in this model are a split and a join (see section 4.4 for more information), inlet and outlet ports and the coupling between them and the main components.

The geometry of the shell and tube condenser can be defined using the parameters listed for the TEMA G shell together with the inner tube diameter, D_i, which is the diameter for the tube model and the number of tube passes, NTP. The condenser model also has parameters for the wall material, medias on the shell and the tube side respectively and initial conditions for the tube side and the shell respectively.

Figure 27: The implementation idea for a multi-pass shell and tube condenser. The thick, grey lines represent the tubes, the half-circles represent the tube bends and the dashed lines represent the shell side control volume.

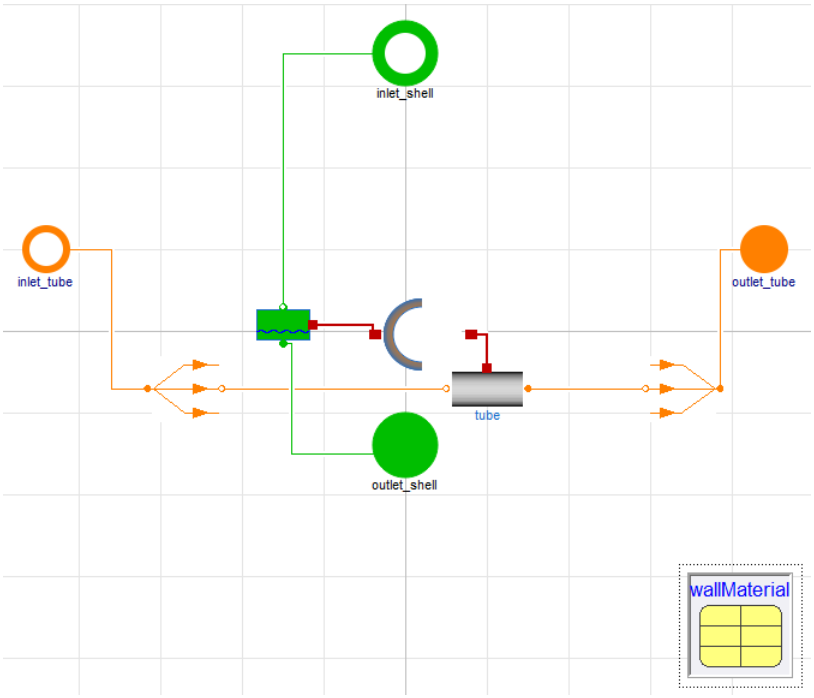

Figure 28: Diagram layer of the condenser model with gas on the tube side.

5 Simulations

5.1 Shell and tube heat exchanger

To be able to perform many tests where only few inputs are changed it is possible to see the effect of one parameter alone. Therefore, the experiments done on the shell and tube heat exchanger model in this thesis used a standard of settings. If nothing else in mentioned in the description of the experiment the standard settings were used. The standard is presented in appendix A.1.

5.1.1 Delaware vs. Modified Delaware

Two methods for pressure drop and heat transfer calculations were implemented and therefore these two correlations were compared. Some interesting quantities to compare are the heat transfer coefficient, the overall pressure drop but also the pressure drop for different sections (the sections are illustrated in figure 5). The standard settings were used except for the correlations on the shell side. The experiment was also done when the shell side mass flow rate was changed to $\dot{m}_s = 5kg/s$.

5.1.2 Varying heat transfer coefficient

In the heat exchanger model the heat transfer coefficient was calculated in each control volume. To control if this was necessary the heat transfer coefficients of the different control volumes were compared. The experiments were conducted using the standard settings, but the experiments were conducted both for the Delaware method and the modified Delaware method.

Apart from comparing the heat transfer coefficients, some comparisons between the fluid properties were made.

5.1.3 Dynamics

The model should be able to handle dynamic boundary conditions, such as increasing mass flow rate. Experiments were executed where dynamic values of the mass flow rate were studied. Specially the mass flow rate was changed so that the coefficients a_{1-4} and b_{1-4} in the Delaware method changed in order to study the development and the effect on important variables. Apart from the changing mass flow rate, standard settings were used.

5.1.3.1 Increasing mass flow In this experiment the mass flow rate on the shell side, $\dot{m}_s$, was increased according to a ramp, see figure 29.

5.1.3.2 Changing coefficients In this experiment the mass flow rate was changed rapidly in order for the coefficients a_{1-4} and b_{1-4} in the Delaware method to change. The mass flow rate used in the experiment is displayed in figure 30.

5.1.3.3 Rapid change To see if the model can handle really rapid changes in the mass flow rate, the input from figure 31 was used. Note that the figure is zoomed in order to see the effect more clearly.

5.1.4 Flow arrangement

Since the model can handle both co-current and counter-current both settings were tested and analyzed. Apart from the flow arrangement, standard settings were used. The inlet and outlet temperatures of the shell and the tubes were compared and from these variable combined with the mass flow rate and specific heat capacity the LMTD correction factor was calculated. Note that the correction factor was never used in the model but only in the analysis on the model.

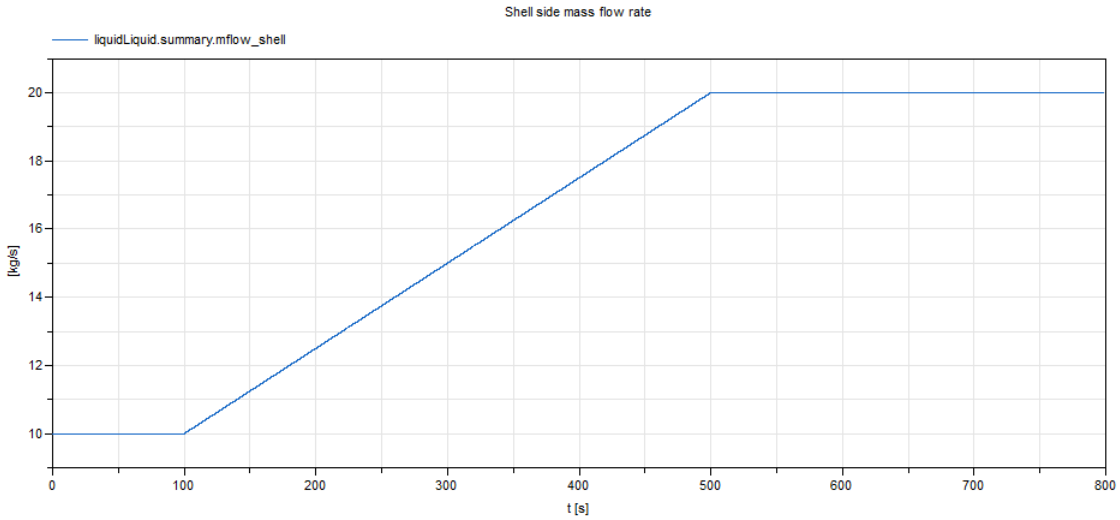

Figure 29: The mass flow rate used in experiment with increasing mass flow rate

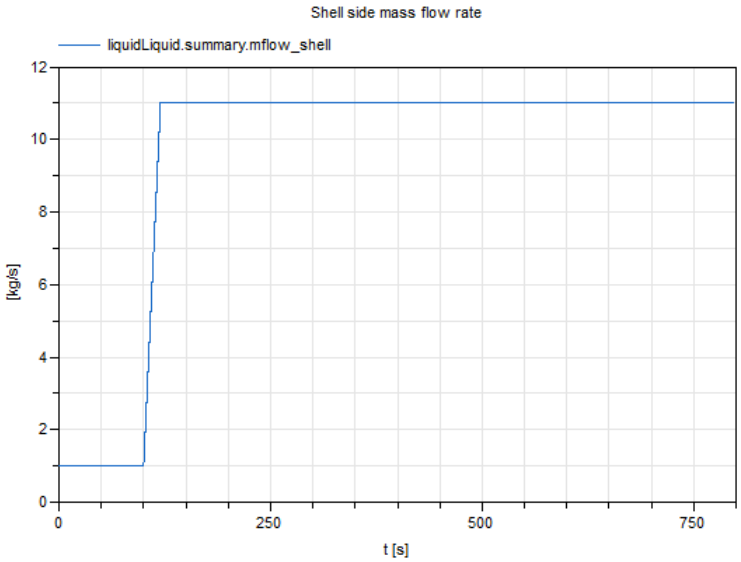

Figure 30: The mass flow rate used in experiment with increasing mass flow rate to change the coefficients in the Delaware method.

5.1.5 Simulation time

To understand the complexity of the implemented model for different geometries the simulation time, the number of equations and the number of continuous time states can be investigated. There are two parameters that define the complexity by deciding the number of control volumes in the shell and the tubes; the number of baffles, n_b, and the number of tube passes, NTP. In this experiment n_b was considered the variable and size of the equation system as well as the simulation time was investigated by changing n_b. In this experiment the standard settings were used except for the number of baffles. The simulation was carried out until $t = 800$ s. The number of time steps were set to 50000 and the tolerance was set to 10^{-4}.

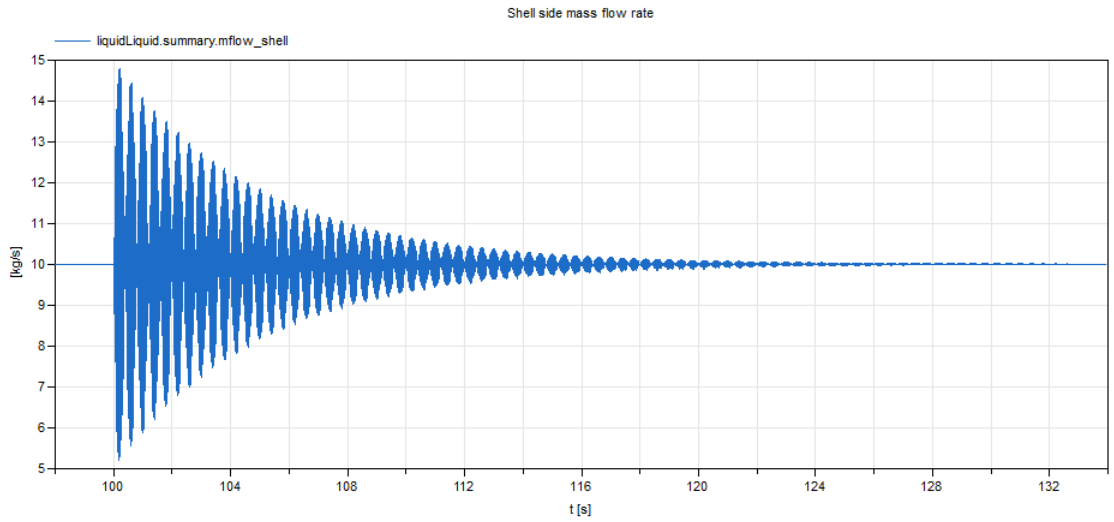

Figure 31: The mass flow rate used in experiment with rapidly changing mass flow rate

5.2 Shell and tube condenser

For the experiments using the implemented shell and tube condenser a standard of settings was used, see appendix A.2. The settings are based on the data provided by Perstorp but modifications were necessary in order to make the model work. This is partly because of missing media models in MBL but mainly because the model does not converge for all geometries and all boundary conditions. If other settings were used in a certain experiment these are given in the description.

5.2.1 Dynamics

To test the dynamical response of the model a varying shell side mass flow rate was used. Both a ramp and a damped sinusoidal function were used as inputs. These are shown in figures 32-33. Standard settings were used except for the mass flow rate on the shell side.

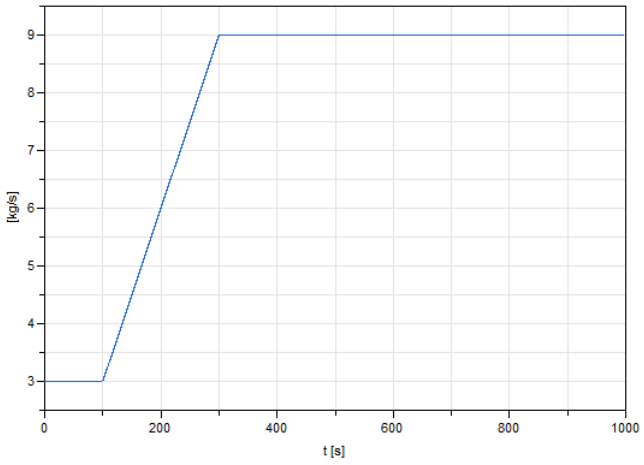

Figure 32: The mass flow rate used in experiment with decreasing shell side mass flow rate

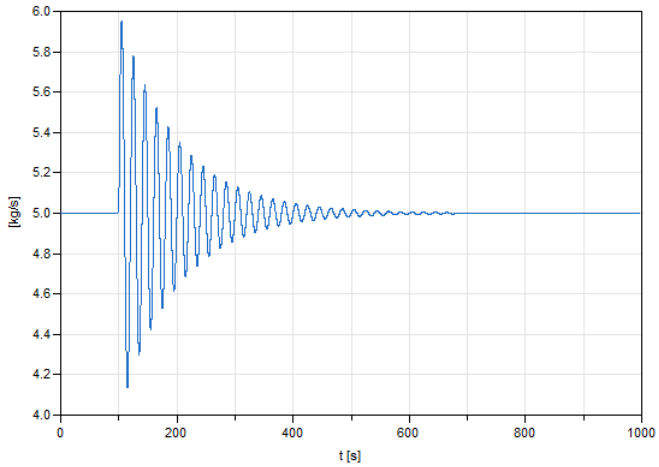

Figure 33: The mass flow rate used in experiment with fluctuating and damped shell side mass flow rate

5.2.2 Mass flow rate effects

As previously mentioned the model does not converge for all cases, for example for different mass flow rates. In this experiment the model was simulated using different mass flow rates to see the effects of it. This was done in two ways. The first was to use one simulation where the mass flow rate was slowly decreased until the simulation no longer converged, the used mass flow rate for this experiment is displayed in figure 34. The second method was to run several simulations with different, constant mass flow rates. The mass flow rates tested were $\dot{m}_s = 5, 4, 3, 2, 1.5, 1.4, 1.3, 1.2, 1.1$ and $1.0\ kg/s$. The standard settings were used except for the mass flow rate on the shell side.

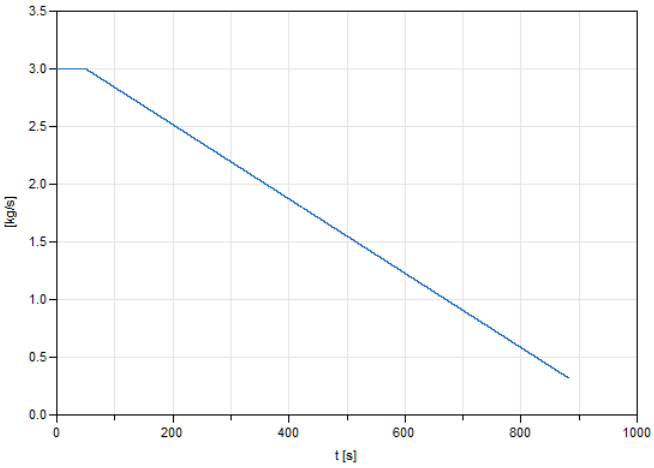

Figure 34: The mass flow rate used in experiment with decreasing mass flow rate until the simulation could not converge.

5.2.3 Liquid level effects

The liquid level is an important variable for the condenser and it decides which components of the shell that the tubes are connected to. Therefore, experiments were conducted to see the effects the liquid level has on the heat transfer. The experiment was done both for water on the shell side and

for R134a (a refrigerant fluid) on the shell side. With water the tube side mass flow rate was changed to $\dot{m}_t = 18\ kg/s$. With R134a on the shell side the number of tube rows were set to 5 (each tube row has four tubes, as in the standard settings), the tube pitches were set to $P_T = P_L = 2.3\ cm$, the inlet enthalpy was set to $h_{s,in} = 430\ kJ/kg$, the outlet enthalpy was set to $h_{s,in} = 300\ kJ/kg$ and the outlet pressure was $p_s = 20\ bar$.

5.2.4 Simulation time

As for the TEMA E shell and tube heat exchanger, tests were done to see the effect on simulation time caused by the number of control volumes. In the condenser model the number of control volumes can be controlled by the number of tube rows, n, and the number of tube passes, NTP. In this experiment the number of tube rows was changed to see the effects on simulation time.

Correlation comparison				
Mass flow:	$\dot{m}_s = 10\ kg/s$		$\dot{m}_s = 5\ kg/s$	
Variable	Delaware	Modified	Delaware	Modified
$\Delta p_{shell}\ [Pa]$	2701.69	3381.39	477.982	872.635
$\Delta p_c\ [bar]$	$6.9 \cdot 10^{-4}$	$9.1 \cdot 10^{-4}$	$2.2 \cdot 10^{-5}$	$2.5 \cdot 10^{-4}$
$\Delta p_w\ [bar]$	$1.8 \cdot 10^{-3}$	$2.1 \cdot 10^{-3}$	$4.4 \cdot 10^{-4}$	$5.3 \cdot 10^{-4}$
$\Delta p_e\ [bar]$	$1.6 \cdot 10^{-3}$	$2.2 \cdot 10^{-3}$	$1.0 \cdot 10^{-4}$	$6.0 \cdot 10^{-4}$
$\alpha\ [W/m^2K]$	3967.2	4844.8	2358.7	2939.9

Table 1: Comparison between the results with the Delaware method and the modified Delaware method respectively.

6 Results

6.1 Shell and tube heat exchanger

6.1.1 Delaware vs. modified Delaware

The different variable documented in the comparison between the two correlations are listed in table 1. In this table, Δp_{shell} is the total pressure drop on the shell side, Δp_c is the mean pressure drop in the cross-flow sections, Δp_w is the mean pressure drop in the window sections, Δp_e is the average between the pressure drop in the enter and the end section and α is the mean heat transfer coefficient.

6.1.2 Varying heat transfer coefficient

In the standard setting the number of baffles was 10, which gave 21 control volumes. The heat transfer coefficient of each control volume is presented in figure 35.

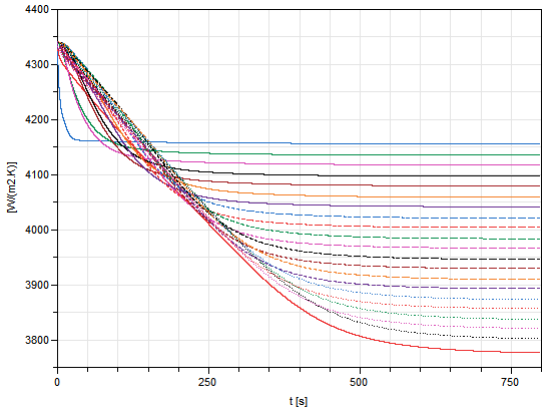

(a) Heat transfer coefficients in the different control volumes for the Delaware method.

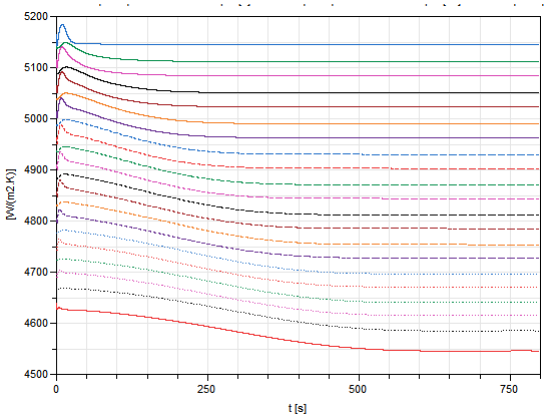

(b) Heat transfer coefficients in the different control volumes for the modified Delaware method.

Figure 35: Heat transfer coefficient in the different control volumes for the respective methods. In both simulations the highest α was in the first control volume and the lowest α was in the last control volume

Since the last control volume had the lowest α and the first control volume had the highest α the values of these CV's are compared. The comparisons between the heat transfer coefficient are displayed in equation 139. The fluid properties used were the thermal conductivity, λ, the dynamic viscosity, η, and the specific heat capacity, c_p were compared for the different control volumes, see equations 140-142.

$$\frac{\alpha_{21}}{\alpha_1} = \begin{cases} \frac{3777.06\ W/m^2K}{4156.54\ W/m^2K} = 0.9087 & \text{Delaware method} \\ \frac{4547.25\ W/m^2K}{5145.22\ W/m^2K} = 0.8838 & \text{Modified Delaware method} \end{cases} \tag{139}$$

$$\frac{\lambda_{21}}{\lambda_1} = \begin{cases} \frac{0.6483\ W/mK}{0.6668\ W/mK} = 0.9723 & \text{Delaware method} \\ \frac{0.6477\ W/mK}{0.6668\ W/mK} = 0.9714 & \text{Modified Delaware method} \end{cases} \tag{140}$$

$$\frac{\eta_{21}}{\eta_1} = \begin{cases} \frac{4.833 \cdot 10^{-4}\ Pas}{3.586 \cdot 10^{-4}\ Pas} = 1.348 & \text{Delaware method} \\ \frac{4.881 \cdot 10^{-4}\ Pas}{3.588 \cdot 10^{-4}\ Pas} = 1.360 & \text{Modified Delaware method} \end{cases} \tag{141}$$

$$\frac{c_{p,21}}{c_{p,1}} = \begin{cases} \frac{4180\ J/kgK}{4190\ J/kgK} = 0.9976 & \text{Delaware method} \\ \frac{4180\ J/kgK}{4190\ J/kgK} = 0.9976 & \text{Modified Delaware method} \end{cases} \tag{142}$$

6.1.3 Dynamics

6.1.3.1 Increasing mass flow rate The resulting shell side pressure drop with increasing mass flow rate (given in figure 29) is shown in figure 36.

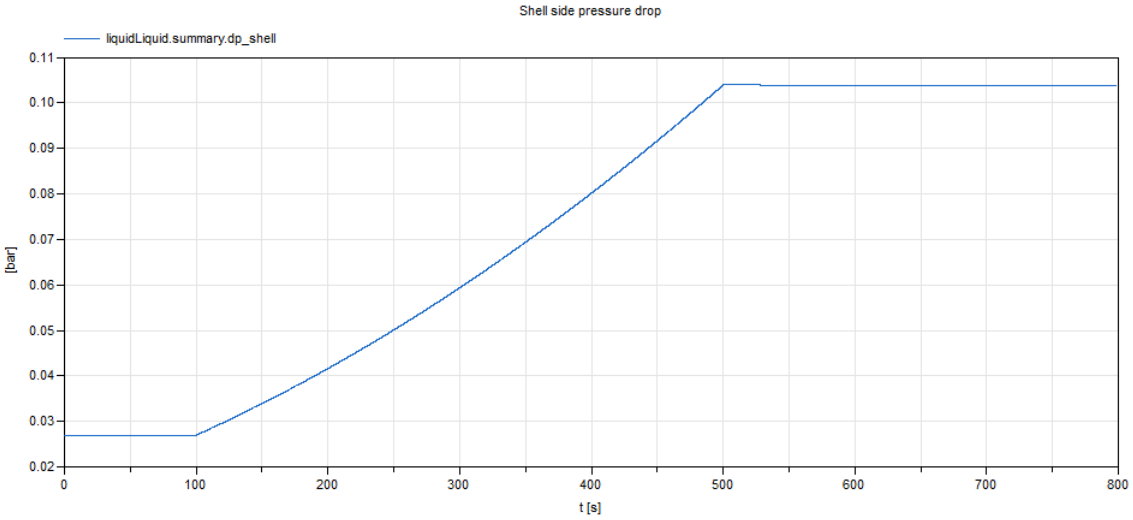

Figure 36: The shell side pressure drop resulting from the increasing mass flow rate

6.1.3.2 Changing coefficients The resulting shell side pressure drop with increasing mass flow rate and changing Delaware coefficients (given in figure 30) is shown in figure 37.

6.1.3.3 Rapidly changing mass flow rate The resulting shell side pressure drop with rapidly changing mass flow rate (given in figure 31) is shown in figure 38.

6.1.4 Flow arrangement

The following values were the results of the simulation with co-current and counter-current respectively, see table 2.

6.1.5 Simulation time

The approximated linear functions were calculated to $t = 2.0826n_b + 5.0175$, $t = 0.0035n_{eq} + 1.8514$ and $t = 0.2603n_{states} + 3.1952$.

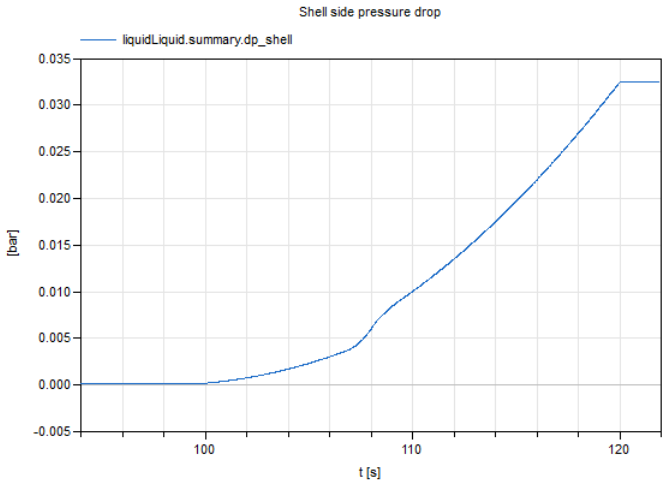

Figure 37: The shell side pressure drop resulting from the increasing mass flow rate and the changing coefficients in the Delaware method

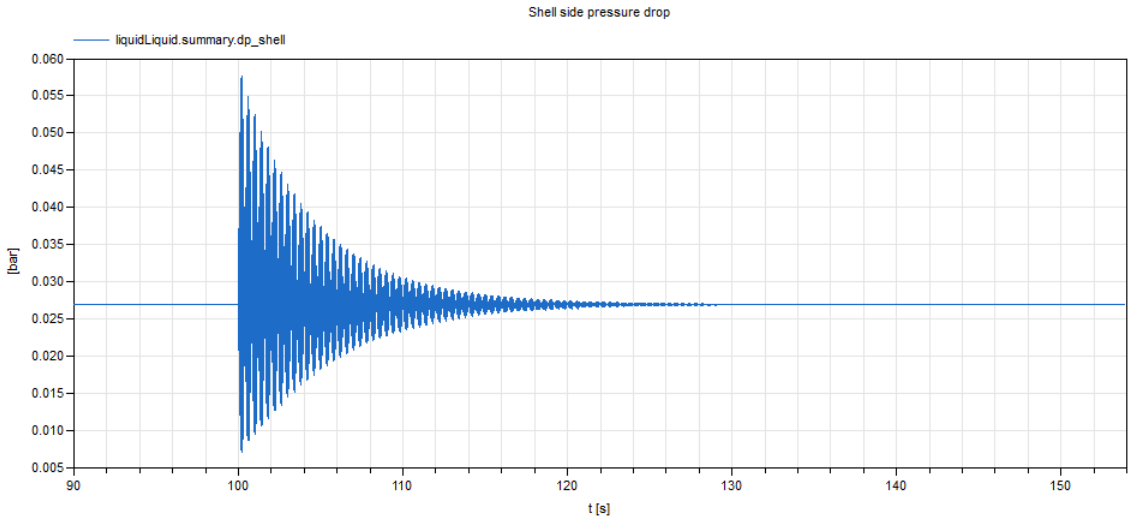

Figure 38: The shell side pressure drop resulting from the rapidly changing mass flow rate

6.2 Shell and tube condenser

6.2.1 Dynamics

The result of the simulation with the mass flow rate given according to figure 32 is shown in figure 40. The result from the simulation with mass flow rate as given in figure 33 is displayed in figure 41. In both these figures the relative liquid level is to the left and the shell side heat flow rate is to the right. Note that it is the relative liquid level that is shown, not the actual liquid level. The relative liquid level is defined as the ratio between the liquid level and the shell diameter.

6.2.2 Mass flow rate effects

Figures 42-45 display the results of the simulation with shell side mass flow rates as defined in figure 34 until the simulation failed. When different, constant mass flow rates were tested the simulation converged without problems for $1.4\ kg/s \leq \dot{m}_s \geq 5\ kg/s$ but for the tests with $\dot{m}_s = 1.3\ kg/s -$

Flow arrangement comparison		
Variable	Counter-current	Co-current
$\dot{m}_s$ $[kg/s]$	10	10
$\dot{m}_t$ $[kg/s]$	10	10
$T_{s,in}$ $[K]$	80	80
$T_{s,out}$ $[K]$	57.44	58.79
$T_{t,in}$ $[K]$	20	20
$T_{t,out}$ $[K]$	42.64	41.23
$c_{p,s,in}$ $[J/kgK]$	4180	4180
$c_{p,s,out}$ $[J/kgK]$	4190	4190
$c_{p,t,in}$ $[J/kgK]$	4180	4180
$c_{p,t,in}$ $[J/kgK]$	4189	4189
Q_{shell} $[W]$	947051	888198
F $[1]$	1	0.948

Table 2: Comparison between the results with counter-current and co-current respectively.

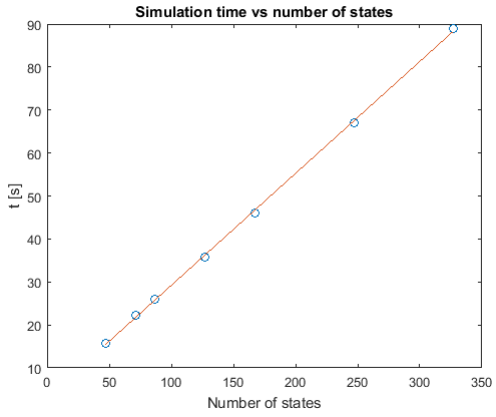

(a) Simulation time as a function of the number of states.

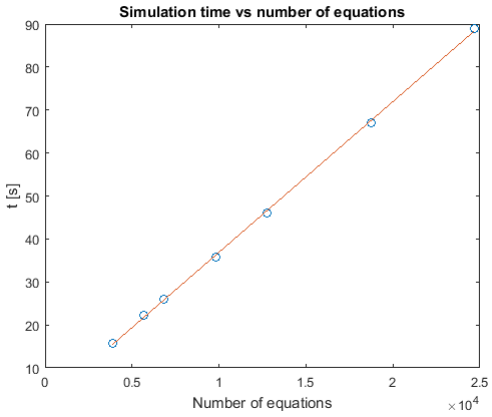

(b) Simulation time as a function of the number of equations.

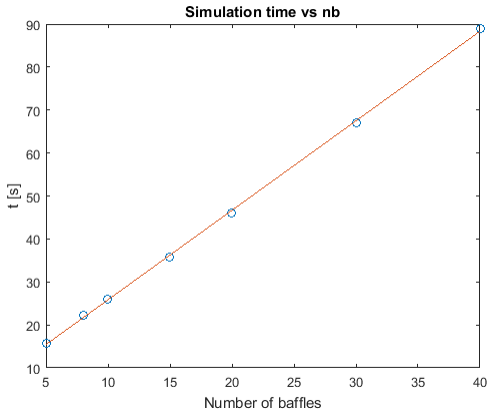

(c) Simulation time as a function of the number of baffles.

Figure 39: Simulation time as a function of the number of states, the number of equations and the number of baffles respectively. The circles are the actual result point and the line is the approximated, linear polynomial.

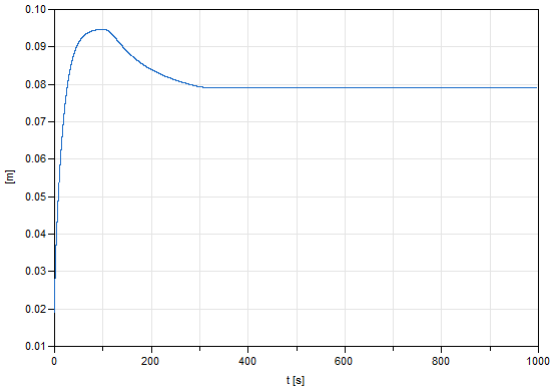

(a) Relative liquid level.

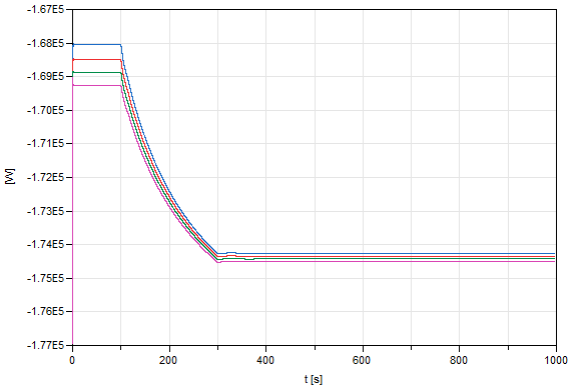

(b) Heat flow rate. The blue, the red, the green and the pink curves correspond to control volumes 1, 2, 3 and 4 respectively.

Figure 40: Result of the simulation with shell side mass flow rate as defined in figure 32.

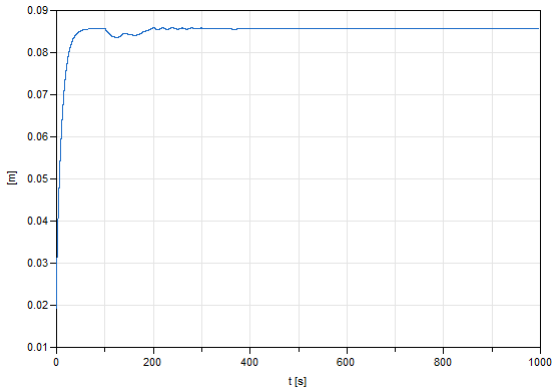

(a) Simulation time as a function of the number of states.

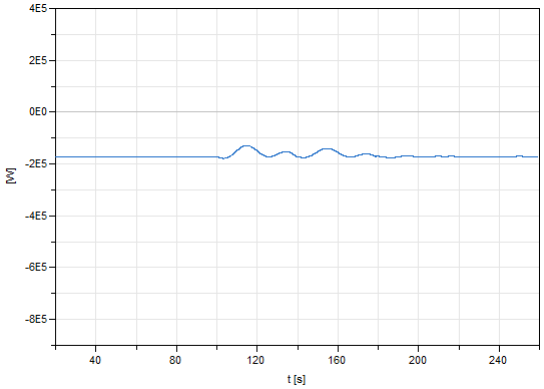

(b) Heat flow rate. The blue, the red, the green and the pink curves correspond to control volumes 1, 2, 3 and 4 respectively.

Figure 41: Result of the simulation with shell side mass flow rate as defined in figure 33.

1.1 kg/s the simulation took longer time (longer time for lower mass flow rate). It was especially the initialization time that was increased. When $\dot{m}_s = 1\ kg/s$ was tested the simulation could not converge.

6.2.3 Liquid level effects

The results of the test on liquid level effect with water on the shell side are displayed in figure 46-47 while the results of the liquid level tests with R134a on the shell side are displayed in figure 48-49. Note that the relative liquid level, not the actual liquid level, is shown. The relative liquid level is defined as the ratio between the liquid level and the shell diameter.

6.2.4 Simulation time

The simulation time is shown in figure 50 as a function of the number of states, the number of equations and the number of tube rows. The test was also done with $n = 9, 11, 12$ but the simulations did not converge.

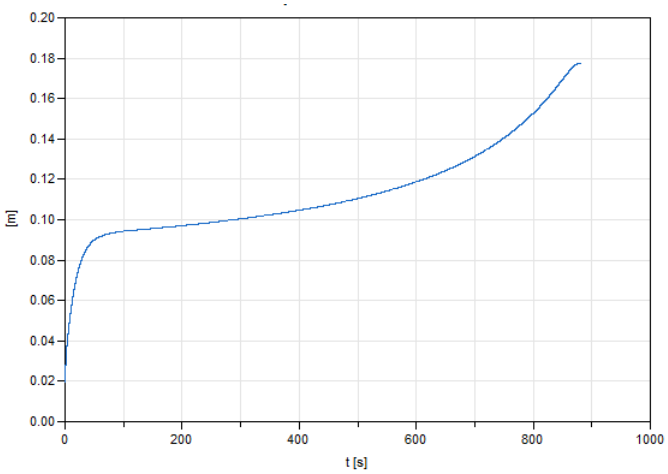

Figure 42: Relative liquid level as a function of time until the simulation no longer converges.

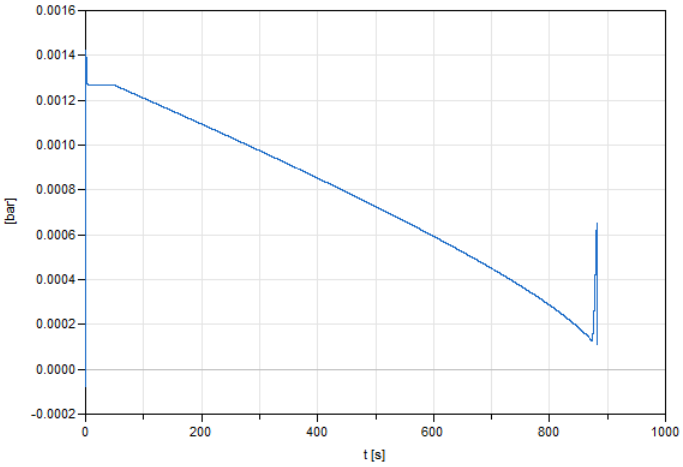

Figure 43: Pressure drop of the condenser pipe (part of the shell) as a function of time until the simulation no longer converges.

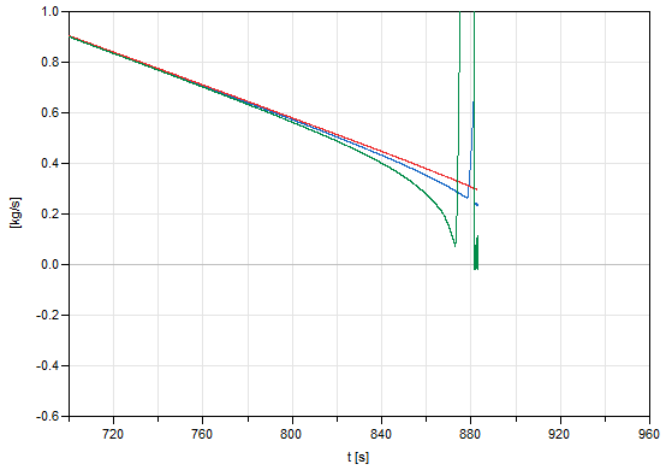

Figure 44: Mass flow rate over the last three control volume boundaries in the condenser pipe (part of the shell) as a function of time until the simulation no longer converges.

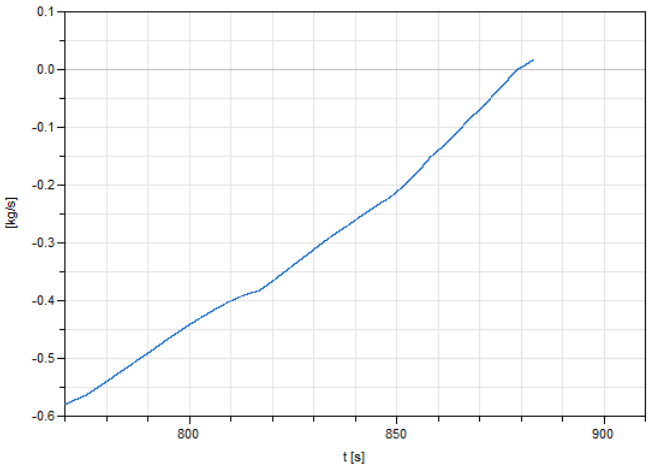

Figure 45: Mass flow rate in the outlet port of the separator component inside the shell as a function of time until the simulation no longer converges.

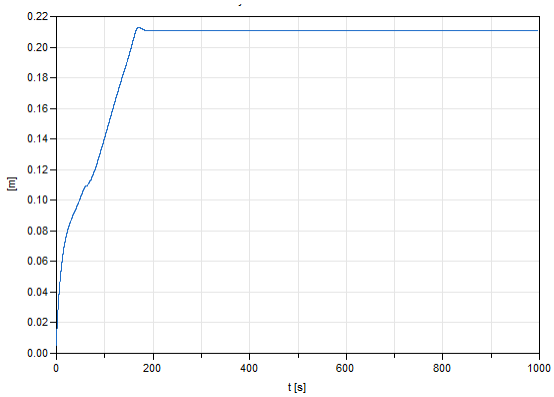

Figure 46: Relative liquid level as a function of time

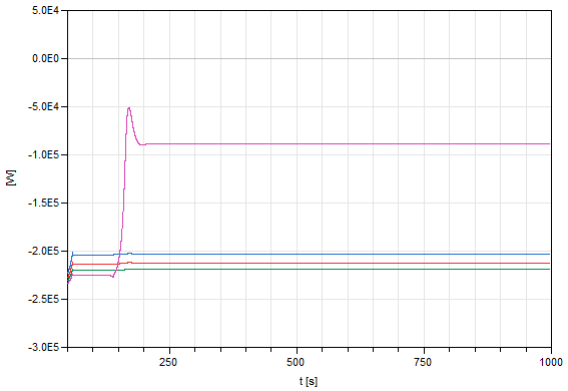

Figure 47: Shell side heat flow rate for the different control volumes. The blue curve is the heat flow rate for the first control volume while the red, the green and the pink curves are the mass flow rates for the second, third and fourth control volume respectively.

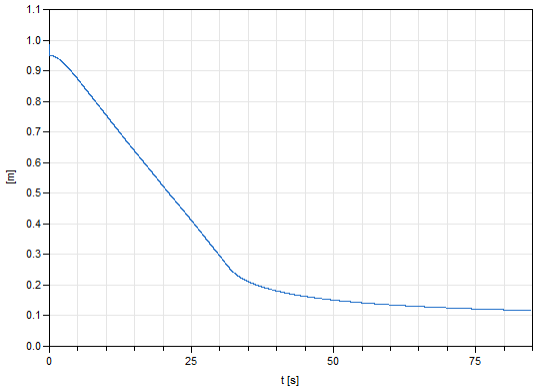

Figure 48: Relative liquid level as a function of time

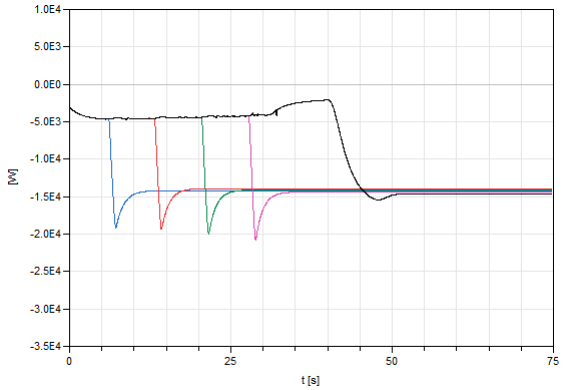

Figure 49: Shell side heat flow rate for the different control volumes. The blue curve is the heat flow rate for the first control volume while the red, the green, the pink and the black curves are the mass flow rates for the second, third, fourth and fifth control volume respectively.

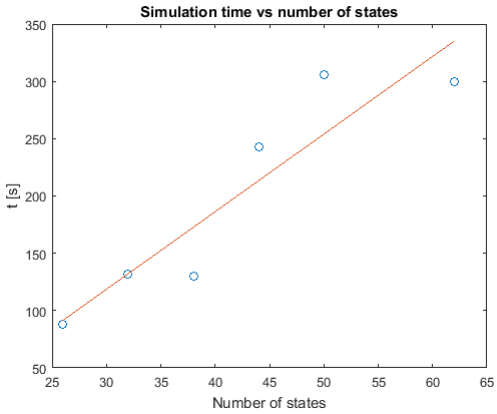

(a) Simulation time as a function of the number of states.

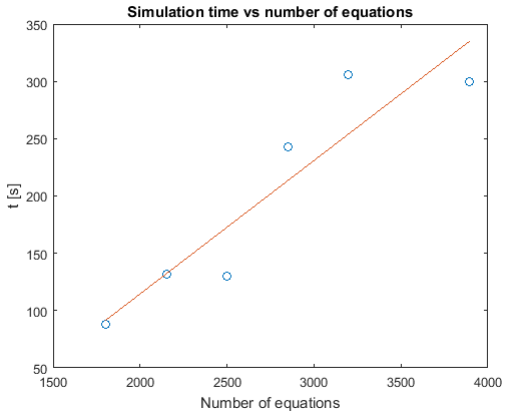

(b) Simulation time as a function of the number of equations.

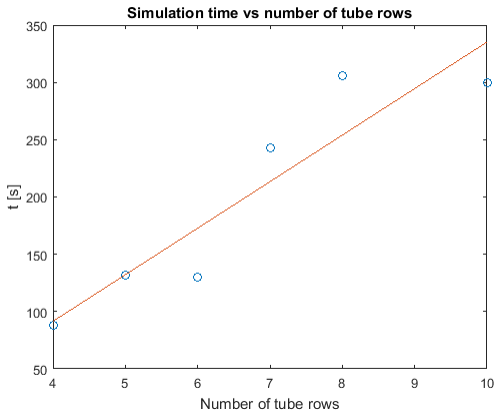

(c) Simulation time as a function of the number of tube rows.

Figure 50: Simulation time as a function of the number of states, the number of equations and the number of tube rows respectively. The circles are the actual result point and the line is the approximated, linear polynomial.

7 Discussion

7.1 Shell and tube heat exchanger

7.1.1 Delaware vs. modified Delaware

Although both correlations used in the single-phase shell and tube heat exchanger are based on the same method, the resulting pressure drops and heat transfer coefficients are significantly different. For both tested mass flow rates, the modified Delaware method calculated both the pressure drop and the heat transfer coefficient to be higher than the Delaware method did. The ratio between α for the two different mass flow rates are similar for the two methods which makes the theory that the modified Delaware method have higher value than the Delaware method for all cases likely, but a firm conclusion of this kind cannot be made without further investigation. In the pressure drop correlations there are more strange differences between the methods. In the simulation with the higher mass flow rate the modified Delaware method estimated the pressure drop to be about 32 % higher than the Delaware method for the cross-flow section and about 17 % for the window section resulting in an overall pressure drop that is about 25 % higher (the pressure drop in the enter and end sections have much less impact since the number of cross-flow and window sections are much higher). When the mass flow rate was $\dot{m}_s = 5\ kg/s$ the behavior was very different. The Delaware method calculated a much higher pressure drop in the window section than in the cross-flow section. The reason for the low cross-flow pressure drop is that the Reynolds number decreases during the simulation due to increased dynamic viscosity as an effect of the decreasing temperature. The Reynolds number decreases slightly below $Re = 10000$ which makes the coefficients b_{1-2} change values. So for this particular mass flow rate the simulation resulted in a switch of the coefficients and the cross-flow pressure drop decreased. Since the same changes in Reynolds number also effect the coefficient a_{1-2} in the heat transfer correlation, the same argument can be used in order to explain why the ratio between α calculated by the modified Delaware method and the Delaware method is higher for the lower mass flow rate, even though this effect is smaller than the effect on the pressure drop.

The dramatic behavior that occurred when the coefficients a_{1-2} and b_{1-2} was changed is a significant property of the Delaware method. The values specified for different ranges of the Reynolds number are practical when only steady-state simulations and when the pressure drop and the heat transfer coefficients are to be calculated by hand. Because no complicated functions have to be used. But in a dynamic simulation the Reynolds number is generally time-dependent which may lead to discontinuities and these are time consuming to solve numerically. This was the main reason for implementing the coefficients using smoothing functions. But a discontinuous behavior is not physical either and this gives reason to question the Delaware method as a suitable method for dynamic simulations. The modified Delaware method also has some equations with different functions depending on the Reynolds number. But these equations are not as important and the limit of the Reynolds number is 100 which is low for a TEMA E shell and tube heat exchanger. Also these equations have smoothing.

To conclude which method is the better would require experimental data. But it is possible to do an analysis of the potential of the two methods. The modified Delaware method can handle any tube layout while the Delaware method only can handle tube layouts of 30^o, 45^o and 90^o. The necessity of implementing other tube layouts than the three mentioned depends on the usage of other tube layouts. An advantage of not having specified tube layout like the Delaware method is that the correlation becomes more general but if only some tube layout is used and if it is possible to assume that no other will be necessary to simulate it can be advantageous to just have these implemented. The reason for this is that the calibration should become easier. If the implemented model should handle tube layout in the range $0 - 90^o$ then more actual heat exchangers have to be tested in order to calibrate the correlation. But if only a fix number of tube layouts are implemented then there is no need to test on other heat exchangers and it might be easier to do a better calibration for the specific tube layouts.

On the matter of calibration both methods have good potential because many coefficients are used that are based on experimental results and not tied to theoretical derivation. These coefficients can

be modified during a calibration.

In conclusion the modified Delaware method has higher potential than the Delaware method because of less discontinuous equations which leads to it being more suited for dynamical simulations and more generality concerning tube layout. But as previously mentioned, this does not mean that the current modified Delaware method delivers more accurate results than the Delaware method.

7.1.2 Qualitative analysis

The dynamical behavior of the model was visualized in figure 36-38. In the first of these figures the mass flow rate was increased slowly and the pressure drop changed correspondingly. No strange behavior can be seen and therefore the conclusion is that the model can handle such an increase of the mass flow rate. To study more dynamical simulations the mass flow rate was increased faster, see figure 29. The change in mass flow rate induced a change in the coefficients in the Delaware method that in theory could be hard for the model to handle since the change is fast. But the resulting pressure drop, shown in figure 37, displays no indications of instability. The pressure drop was increased smoothly but the transition between the two states of the coefficients is clear at around $t = 108\ s$. To increase the difficulty for the model, the mass flow rate was set to a damped sinusoidal function, see figure 31. According to figure 38 the model seems to be responding well. Overall the model seems good at handling dynamical simulations.

If the mass flow rate effects are further investigated, perhaps some conclusions concerning the pressure drop model can be drawn. Since most pressure drop correlations (including part of the Delaware method) have a relation between the mass flow rate and the pressure drop according to $\Delta p \sim \dot{m}^2$, the pressure drop should be multiplied by four when the mass flow rate was doubled which was the case for the slowly increasing mass flow rate. But in this case the ratio between the pressure drop in the end and in the beginning of the simulation was around 3.85. In the simulation when the mass flow rate was changed according to figure 30 the mass flow rate was multiplied by 11 which means that the pressure drop would be multiplied by 121. Although in figure 37 the ratio could be calculated to around 168, clearly higher. Both simulation show that the pressure drop is not quadratically dependent on the mass flow rate but it is on the same order of magnitude.

One reason to compare the heat transfer coefficients of the different control volumes is to investigate whether it is necessary to compute a heat transfer coefficient in every control volume or if only one calculation could be made in order to reduce the number of equations. In figure 35 it is clear that the heat transfer coefficient varies along the heat exchanger, for both correlations. For the Delaware method, α in the last CV was about 91% of the α in the first CV and for the modified Delaware method the same number was around 88%. Some reasons for this were investigated in section 6.1.2. Three fluid properties were analyzed and their value in the last CV was compared with their value in the first CV. For the thermal conductivity, λ, the ratio was around 97% for both correlations. For the dynamic viscosity, η, the value in the last CV was 135 % for the Delaware method and 136 % for the modified Delaware method. The ratio of the specific heat capacity was almost one for both correlations. The variations of the heat transfer coefficients are too large to ignore. Together with the knowledge that the fluid properties changes, especially the dynamic viscosity, this gives reason to do the calculations in each CV. But in figure 35 the heat transfer coefficients of all CV's are shown. When the simulation had reached steady-state the heat transfer coefficients appears to be equidistant which means that the medium heat transfer coefficient probably is close to the average of the first and last heat transfer coefficient. For the Delaware method this can be tested using table 1. The mean heat transfer coefficient is $\alpha = 3967.2\ W/m^2K$ and the average between the heat transfer coefficient in the first and the last CV is $\alpha = 3966.8\ W/m^2K$ (values taken from equation 139). This is very close which means that computing the heat transfer coefficient in the first and the last CV might be a good way to approximate the mean heat transfer coefficient. But there are clear disadvantages of doing so. First of all, the change in fluid properties is significant and it may not be linear which would make an averaging dangerous. Secondly the Reynolds number is dependent on the fluid properties and the dependency on the dynamic viscosity is not linear. This would introduce errors in the Reynolds number and since the heat transfer coefficient is highly depending on the Reynolds number the errors

would be introduced to the heat transfer coefficient as well. This effect would be extra dramatic in the Delaware method since an error in the Reynolds number might lead to a change in the coefficients a_{1-2} which would create major error in the heat transfer coefficient. Thirdly the heat transfer coefficient in the different CV's are only approximately equidistant in the steady-state case. Earlier in the simulation the relations between the values are more complex. Since the model should be able to use for dynamical simulations the heat transfer coefficient should not be computed as an average.

To test the different flow arrangements is good since the counter-current heat exchanger is known to be better than the co-current. This was also the case for the model, as shown in table 2. The fact that the counter-current model is better can be seen by observing the outlet temperatures and the heat flow rate. The outlet temperature of the shell side (which is the hot side) is lower and the outlet temperature of the tube side (which is the cold side) is higher for the counter-current heat exchanger. This means that more heat was transferred to the cold side from the hot side which is good since this is the purpose of a heat exchanger. The fact that more heat was transferred in the counter-current heat exchanger could be seen when observing the heat flow rate as well. The value is around 6.6 % higher for the counter-current heat exchanger than for the co-current heat exchanger. This difference is significant and demonstrates that the model is capable of modelling the difference between the two flow arrangements. The modelling of the different flow arrangements was done by connecting the tube wall to the shell differently depending on the flow arrangement. Therefore, the result in table 2 can be used to argue that the connection between the shell and the tube wall works in a good fashion.

The relation between the number of baffles and the simulation time was investigated in order to see the effects of increasing the size of the system. The relation is clearly linear, as shown in figure 39c. All data points are very close to the approximated line which concludes that the relation is linear and that the simulations of larger shell and tube heat exchangers are more time-consuming. The time was also plotted against the number of equations and the number of time states. This was partly done to see if these relations also were linear but also to see the actual sizes of the systems, since the data points in the three subplots in figure 39 are taken from the same simulations. The fact that the number of states relates to the number of baffles as $n_{states} = 8n_b + 7$ could already be seen in Dymola since Dymola prints the chosen time states. It is hard to conclude if the system is large since that is relative but the time it takes to simulate a shell and tube heat exchanger model with up to 40 baffles for 1000 seconds is fairly low.

7.1.3 Weaknesses of the model

Even though the model works in a good fashion it has some weaknesses that needs to be discussed.

The heat transfer and pressure drop correlations shown different results which means that either one or both of them is wrong. This is a disadvantage since a user probably can be assumed to not know which one of the methods is better for their experiments. Both correlations could be calibrated using experimental data but until they are the question on which method to use remains.

The model only handles TEMA E shell and tube heat exchangers with single-phase flow on the shell side. The model could be expanded to handle evaporation (for example by using the method developed by Gavin H. Doo [12]) and condensation (for example by using the Honda method) but besides heat transfer and pressure drop correlations models for two-phase flow needs to take special care of outlets and inlets since the flow is more complicated. The implemented model could also be expanded to other shell configurations than the ones considered in this thesis but for some configurations this would require other models for heat transfer and pressure drop and other geometrical parameters would be defining the shell.

The shell model assumes single-segmental baffles and unfinned tubes which is not always the case for shell and tube heat exchangers. These assumptions were made because the Delaware method and the modified Delaware method make these assumptions. If other type of baffles or finned tubes would be implemented, other correlations would be required. But since the shell side discretization also assumes single-segmental baffles another discretization might have to be used for other types of baffles. This would significantly increase the difficulty of the modelling and for that reason it was not done in this thesis.

The shell and tube heat exchanger model does not include heads and nozzles which have an impact on a real heat exchanger. This makes is harder for a user to analyze the result of simulations.

A real heat exchanger has losses. For example, heat can travel from the shell to the surrounding environment, decreasing the heat inside the heat exchanger. How large the losses are depends on several properties of the heat exchanger. For example, the thickness of the shell wall which decides the thermal resistance, much like it does for the tube wall. A thicker shell wall would lead to lower losses. It also depends on the shell medium and the Reynolds number of that medium since these properties are used to calculate the heat transfer coefficient. And the heat transfer coefficient is one of the difficulties if losses were to be introduced. If the losses would be calculated using the temperature difference between the shell wall and the surroundings and the temperature difference between the shell wall and the shell fluid correlations would be required for the heat transfer coefficients on both sides of the shell wall.

7.2 Shell and tube condenser

7.2.1 Qualitative analysis

Without doing a numerical comparison to a real heat exchanger it is possible to study and analyze the behavior of the model.

There are some advantages with using a condenser. One is that the enthalpy of the fluid can be decreased without the temperature decreasing. This is a good quality because the heat flow rate is dependent on the temperature difference between the fluids. The second property of a condenser is the high heat transfer coefficient in the two-phase section. A large heat transfer coefficient leads to high heat flux. The liquid level is therefore an important variable for a condenser. If the liquid level is above a tube, that tube will not interact with the two-phase region of the shell and the heat flux will be smaller than for the tubes in two-phase region of the shell. This effect was caught by the condenser model. In figure 48 the relative liquid level (liquid level divided by the diameter) is displayed. It starts high because of the initial condition in the receiver. But as the simulation progress the level sinks because the liquid exits the shell and gas is coming in. The exit vapor quality, x_{out}, is implemented as a function of the liquid level which means that a high liquid level results in a low vapor quality, more liquid. This means that the high liquid level results in much liquid leaving the receiver. This explains the effects in figure 48. When the liquid level decreases x_{out} increases and therefore the liquid level is stabilized on a steady-state level. The heat transfer effect of the liquid level can be seen in figure 49. As predicted, the heat flow rate was strongly increased when the liquid level sank below a tube row. It is also possible to observe the smooth transition between the two heat transfer connections. This smoothing was done for two reasons. The first was to avoid numerical problems that discontinuous functions may lead to. The second reason was that it is unlikely that a discontinuous switch between two states is realistic. Especially considering that the tubes are not line-shaped but shaped as cylinders. As the lower part of the tube sinks below the liquid level the upper part might still be above. It might be possible to come up with a smoothing or transition function that describes this behavior but both for the simplicity of implementing and the lack of knowledge of such a transitions function, a simple splice function was used. The effect of the liquid level can be seen more clearly in figures 46 and 47. Here the liquid level rises from zero to a level within the transition zone of the lowest tube row, after peaking the level was stabilized at a level slightly above 0.2 (the position of the lowest tube row). Why does the liquid level peak? One explanation could be that as the liquid level rises above the tube level the heat flow rate is decreased. Decreased heat flow rate in the condenser pipe means that less vapor will condense to liquid which means that the liquid level will decrease.

Another way to do a qualitative analysis of the model is to see how the model reacts to changed mass flow rate. For this purpose, the mass flow rate was changed from $\dot{m}_s = 3\ kg/s$ to $\dot{m}_s = 9\ kg/s$. The resulting effects on the liquid level and the heat flow rate are visualized in figure 40. In this figure it is possible to see that increased mass flow rate led to lower liquid level and higher heat flow rate. Is this reasonable? The increasing heat flow rate is logical because higher mass flow rates results in

higher velocity on the shell side, which usually is connected to higher heat transfer coefficient. But if the relative changes in figure 40b are observed the conclusion is that those are much smaller than the relative changes in mass flow rate. This means that only slightly more heat is transferred to three times more mass. This should lead to less of the fluid being condensed which is the reason for the decreased liquid level in figure 40a.

When the mass flow rate was given as a damped sinusoidal function the resulting heat flow rate almost resembled the same type of function, see figure 41b. But the heat flow rate does not look quite like the mass flow rate. A reason for this is that as the heat flow rate changes, the tube wall temperature changes as well. This means that the temperature difference between the shell and the tube wall changes and this effects the heat flow rate, making it not look like the mass flow rate. It is also interesting to see that the liquid level, presented in figure 41a look even less like the shape of the mass flow rate. First of all, the liquid level is a function of many different elements in the heat exchanger and not only effected by the mass flow rate. Secondly, the liquid level is a result of the simulation also before the changed mass flow rate. In theory the heat flow rate could be changed discontinuously if the mass flow rate also is, but this is not the case for the liquid level since it would require an infinite amount of heat to condense an amount of the fluid in zero time. This can be compared to a car getting increased force from the motor. If the increase of the force is discontinuous then so can the acceleration be, at least in theory. But the velocity cannot change discontinuously since that would require an infinite amount of force and thereby an infinite amount of energy. It should also be recalled that the liquid level is not proportional to the liquid volume because of the shape of a cylinder.

Overall the tests on the condenser model show several behaviors that would be expected for a real condenser. To make a quantitative analysis, experimental data would be required. But the model shows good potential to correspond to a real shell and tube condenser.

7.2.2 Weaknesses of the model

As most models, the shell and tube condenser model has weaknesses. One of the most obvious is that the model cannot handle too low mass flow rates on the shell side, this can be seen in figure 34. When the mass flow rate is about $\dot{m}_s = 0.3\ kg/s$ the simulation fails. To know what causes this failure other variables can be observed. The liquid level for the same experiment is displayed in figure 42. Nothing drastic seems to happen with the liquid level that could cause simulation failure. But figure 43 show dramatic changes in the pressure drop in the condenser pipe at the end of the simulation. The question is if this is the cause of the simulation failure or an effect of something else that behaves strange. The pressure drop is dependent on the mass flow rate and in figure 44 is it clear that the mass flow rate in the condenser pipe also have a strange behavior. But it is only the two last mass flow rate that appear strange. The red line is still straight. One possible explanation for these curves could be found in figure 45. Here the mass flow rate in the outlet port of the separator is shown. Just before $t = 880s$ the mass flow rate becomes positive. This means that the fluid travels through the outlet in to the condenser instead of the reverse. A problem could therefore be that the model does not handle reverse flow in a proper manner. But the instabilities in figure 44 cannot only be explained by the reverse flow in the outlet of the separator since the time of the instability is about $t = 873\ s$, earlier than the back-flow. It would therefore appear as if the pressure drop correlation in the model gives unstable mass flow rates. As the mass flow rate changes dramatically the coefficient b_{1-2} will also change. Since these coefficients are used to calculate the mass flow rate this might lead to an unstable correlation. One way to change this would be to change the pressure drop correlations used in the model. Another way would be to analyze the handling of reverse flow. An analysis would include the physical meaning of flow into the receiver from the outlet.

The discussion on the outlet of the receiver can lead to a discussion on one of the modelling assumption for the TEMA G shell: The vapor and the liquid have the same outlet. In the separator (part of the receiver model) the liquid level is calculated and depending on this liquid level the outlet vapor quality can be calculated. But is it realistic that vapor exits the receiver despite the liquid level being above zero? Perhaps it would be more reasonable to have one outlet for the vapor and one for

the liquid. Or an outlet where the vapor quality always is zero (liquid only). In the latter the idea is that the vapor stays in the shell until it is condensed.

This reasoning leads into another modelling question: Is it good to have one receiver and one condenser pipe in the shell model? The idea of this was to calculate the liquid level as a function of the fraction of the volume covered by liquid. But the volume fraction, V_{liq}, is calculated using the thermodynamic state in the receiver, after the entire condenser pipe. The difficult problem with calculating the liquid level as a function of the state in the condenser pipe is that the condenser pipe consists of several control volumes, with a different state in each control volume. Which thermodynamic state would be used? A different approach to this problem would be a moving boundary modelling. In this case the shell would be divided into a liquid part and a two-phase part. The boundary between the parts would be able to move depending on the liquid level. This method would likely be more numerical and would require another kind of modelling but to account for the effects of the liquid level this could be a preferable method.

Some experiments on the shell and tube condenser model show problems in the initialization. This appears both when different, constant mass flow rates are given as boundary conditions and when different number of tube rows are tried, see figure 50. When the mass flow rate was $\dot{m}_s = 1.4 - 5\ kg/s$ no problems appeared in the initialization but when this number was decreased to 1.1 the initialization time was increased and when $\dot{m}_s = 1\ kg/s$ the solver could not initialize. This could have to do with inconsistent initial conditions. The problems regarding initialization could also be found when the number of tube rows where increased, see figure 50. It is reasonable that the initialization time, as well as the total simulation time, should increase as the system gets bigger but the effects are clearly not linear and that could mean that some geometries and initial conditions are harder to simulate. It is hard to know the reason for this but a solution might be to specify initial conditions more carefully.

As two of the most important variables of the model, the heat transfer coefficient and the pressure drop, is calculated using correlations built on experiments the model can only be as good as the correlations. Even though the correlations themselves have been experimentally tested the model using them should be calibrated according to data from a real shell and tube condenser to make the calculations adjusted to reality. The Honda method, used in the condenser pipe, has the disadvantage of being implicit. The Nusselt number is dependent on the heat flux which is dependent on the Nusselt number. Implicit equations are used in more two-phase heat transfer correlations [2]. Having implicit equations increases the complexity of the simulations and make it harder to locate the source of an instability. But the implicit equations may be necessary in order to model the heat transfer correctly and for the reason they are not always possible to avoid without losing accuracy.

7.3 Conclusion

In this thesis a TEMA E shell and tube heat exchanger with single-phase flow on the shell side was modelled. The modelling was done in Modelica by creating models for the different sub-components and connecting them to each other.

The modelling of the shell and tube heat exchanger was successful. The simulation time was reasonable and the methods used have been developed based on experimental results, although the two methods did not calculate the same heat transfer coefficient and pressure drop.

By using different mass flow rates on the shell side a qualitative analysis was done. Increased mass flow rate induced an increase in pressure drop as is expected. The relation between the mass flow rate and the pressure drop was compared with $\Delta p\ \dot{m}^2$ and the conclusion was that the calculated pressure drop was on the same order as this relation would suggest but it deviated enough to conclude that the correlation is more complex than a simple quadratic. The stability of the model was also tested using varying mass flow rates. Partly by linearly increasing the mass flow rate in order to change the coefficients in the Delaware method and partly by having a highly fluctuating mass flow rate. The transition between two values of the coefficients was done well and it was clearly seen in the corresponding graph for the pressure drop. The highly fluctuating mass flow rate resulted in a highly fluctuating pressure drop as was expected and the simulation was stable.

The difference between counter-current flow and co-current flow could be seen in the simulations which makes it probable that the shell model, the tube wall model and the tube model were connected in a good fashion.

The heat transfer coefficient in the different control volumes were compared and the possibility of not calculating the heat transfer coefficient in every control volume in order to reduce the number of equations was discussed. The conclusion was that the heat transfer coefficient needs to be calculated in every control volume since the difference in fluid properties was too high and the error a simplification might cause was too large.

Some weaknesses of the model involve the lack of implementation of heat losses to the environment surrounding the heat exchanger, the fact that both single-segmental baffles and unfinned tubes were assumed and that no calibration was done.

A model of a TEMA G shell and tube condenser was also created in this thesis. In a similar fashion as the TEMA E shell and tube heat exchanger the condenser model was constructed by connecting models for the shell, the tube wall and the tube.

The modelling of the shell and tube condenser was more complex than the modelling of the TEMA E heat exchanger and problems occurred during simulation of certain cases, for example when the mass flow rate was too low. The simulation time was significantly higher than for the single-phase shell and tube heat exchanger with equal number of equations which partly was the consequence of implicit system of equations for the heat transfer and pressure drop correlations.

Even though some geometries and boundary conditions did not work for the condenser model, general results from simulation that did converge could be analyzed. The liquid level effects appeared and had a great impact on the heat flow rate. The heat transfer coefficient was much higher in the condenser pipe of the shell than in the shell receiver which implies that the heat flow rate is higher for a tube row above the liquid level. The transition from heat transfer from the receiver to heat transfer from the condenser part was not a problem for convergence, it was done smoothly.

Mass flow rate effect were also studied. Increased mass flow rate on the shell side led to higher heat flow rate and lower liquid level, as was expected.

Even more than the TEMA E shell and tube heat exchanger the condenser model suffer from lack of calibration since the models for heat transfer and pressure drop were not developed specifically for the heat exchanger it was used on in this thesis, unlike the models for the TEMA E. The condenser model miss modelling of heat leakage as well as the TEMA E heat exchanger.

7.4 Future work

The first idea on continuation of this thesis is the implementation of a model of a shell and tube condenser that works for all applicable geometries and boundary conditions. This could either be done by extension of the model created in this thesis or by working on another approach, for example the moving boundary method. This method certainly has potential to account for the effect of the liquid level and the ideas of coupling between the different sub-components from this thesis could be reused.

Since only two different kinds of models were created in this thesis one idea of future work could be to model different shell configurations and different phase configurations. For some of the shell and tube heat exchangers not yet modelled several modelling ideas from this thesis could be reused, for example the shell side discretization.

Calibrating the existing methods would be a good way to improve the models and justify the modelling methods that are used.

8 References

References

[1] Wikipedia. *Värmeväxlare*. URL: https://sv.wikipedia.org/wiki/V%C3%A4rmev%C3%A4xlare.

[2] B. Sundén. *Introduction to heat transfer*. WITpress, 2012.

[3] R. W. Serth and T. G. Lestina. *Process heat transfer, second edition*. Elsevier Inc, 2014.

[4] Wikipedia. *Shell and tube heat exchanger*. URL: https://en.wikipedia.org/wiki/Shell_and_tube_heat_exchanger.

[5] R. K. Shah and D. P. Sekulic. *Fundamentals of heat exchanger design*. John Wiley and Sons, Inc, 2003.

[6] TEMA. *Standard Tubular Exchanger Manufacturers Association, eight edition*. Tubular Exchanger Manufacturers Association, Inc, 1999.

[7] Sadik Kakac. *Heat exchangers - selection, rating and thermal design*. 1999.

[8] Martin Otter. *Modelica overview*. URL: https://www.modelica.org/education/educational-material/lecture-material/english/ModelicaOverview.pdf.

[9] *Modelon Modelica Libraries*. Nov. 5, 2016. URL: http://www.modelon.com/products/modelica-libraries/.

[10] *VDI Heat Atlas, second edition*. Springer, 2010.

[11] Uday V. Shenoy. *Heat exchanger network synthesis*. Gulf publishing company, 1995.

[12] Gavin H. Doo. *A Modelling and Experimental Study of Evaporating Two-Phase Flow on the Shellside of Shell-and-Tube Heat Exchangers*. University of Strathclyde, 2005.

[13] J. G. Collier and J. R. Thome. *Convective boiling and condensation, third edition*. Oxford University Press Inc, 1994.

[14] F. M. White. *Fluid mechanics, seventh edition in SI units*. McGraw-Hill Education, 2011.

[15] R. K. Shah. *A general correlation for heat transfer during film condensation inside pipes*. 1979.

[16] H. A. Deans W. W. Akers and O. K. Crosser. *Condensing heat transfer within horizontal tubes*. 1959.

[17] J. R. Thome. *Two-Phase Heat Transfer to New Refrigerants*. 1994.

[18] S. G. Kandlikar. *A general correlation for saturated two-phase flow boiling heat transfer inside horizontal and vertical tubes*. 1990.

[19] K. E. Gungor and R. H. S. Winterton. *Simplified general correlation for saturated flow boiling and comparisons of correlations with data*. 1987.

[20] J. C. Chen. *Correlation for boiling heat transfer to saturated fluids in convective flow*. 1966.

[21] L. Cheng and T. Chen. *Comparison of Six Typical Correlations for Upward Flow Boiling Heat Transfer with Kerosene in a Vertical Smooth Tube*. 2000.

[22] L. Friedel. *Improved Friction Pressure Drop Correlations for Horizontal and Vertical Two-Phase Pipe Flow*. 1979.

[23] C. Y. Park and P. S. Hrnjak. *CO 2 and R410A Flow Boiling Heat Transfer, Pressure Drop, and Flow Pattern at Low Temperatures in a Horizontal Smooth Tube*. 2007.

[24] C. Y. Park and P. S. Hrnjak. *CO 2 Flow Condensation Heat Transfer and Pressure Drop in Multi-Port Microchannels at Low Temperatures*. 2009.

A Heat exchanger geometry

A.1 Standard settings for the tests of the shell and tube heat exchanger

Standard values	
Choice	Setting
Heat exchanger type	LiquidLiquid
Wall material	Aluminum
Shell medium	Water
Tube medium	Water
Shell side correlation	Delaware
Tube side friction	Detailed wall friction
Tube side heat transfer	Gnielinski
Flow arrangement	Counter-current
Tube layout	In-lined
D_s	0.48 m
n_b	10
B	0.3 m
B_{in}	0.3 m
B_{out}	0.3 m
B_c	0.25
δ_{sb}	$1.04{\cdot}10^{-3}$ m
N_{ss}	1
D_{otl}	0.45 m
δ_{tb}	$4{\cdot}10^{-4}$ m
n_t	110
n_w	30
NTP	1
D_o	$2.54{\cdot}10^{-2}$ m
D_i	$2.2{\cdot}10^{-2}$ m
P_T	$3.2{\cdot}10^{-2}$ m
P_L	$3.2{\cdot}10^{-2}$ m
N_c	10
N_cw	5
N_t	5
$\dot{m}_s$	10 kg/s
$\dot{m}_t$	10 kg/s
$T_{s,in}$	80 ^oC
$T_{s,out}$	60 ^oC
$T_{t,in}$	20 ^oC
$T_{t,out}$	40 ^oC

Table 3: Standard settings for the experiments on the shell and tube heat exchanger model.

A.2 Perstorp condenser and the standard settings in the simulations

One of the settings (both geometrical and boundary conditions) for the shell and tube condenser tests was taken from a real condenser, owned by Perstorp.

Standard values		
Choice	Perstorp	Used
Shell medium	Water	Water
Tube medium	Gas (H_2, N_2, CO)	Air
Tube layout	Staggered	Staggered
D_s	0.63 m	0.63 m
NTP	1	1
D_o	$2{\cdot}10^{-2}$ m	$2{\cdot}10^{-2}$ m
D_i	$1.7{\cdot}10^{-2}$ m	$2{\cdot}10^{-2}$ m
P_T	$2.5{\cdot}10^{-2}$ m	$2.5{\cdot}10^{-2}$ m
p_{out}	14 bar	14 bar
Number of tube rows	27	4
Number of tubes	514	16
$\dot{m}_s$	0.114 kg/s	5 kg/s
$\dot{m}_t$	0.611 kg/s	10 kg/s
$h_{s,in}$	2600 J/kg	2600 J/kg
$h_{s,out}$	800 J/kg	2100 J/kg
$T_{t,in}$	60 ^oC	-10 ^oC
$T_{t,out}$	130 ^oC	50 ^oC
Wall material	Stainless steel	Aluminum

Table 4: Standard settings for the experiments on the shell and tube condenser model compared to the settings of the real condenser from Perstorp.